PREDICTION METHODS FOR POOL BOILING HEAT TRANSFER:

A STATE-OF-THE-ART REVIEW(*)

Dieter Gorenflo[(a)], Elmar Baumhögger[(a)], Gerhard Herres[(a)],

and Stephan Kotthoff[(b)]

[(a)]Thermodynamik und Energietechnik, Fakultät für Maschinenbau, Universität Paderborn,
33098 Paderborn, Germany, mailto:digo@thet.upb.de
[(b)]Siemens AG, 02826 Görlitz, Germany

(*) Extended version of a keynote lecture held at 4th IIR Conf. on Thermophysical Properties and Transfer Processes of Refrigerants, Delft, The Netherlands, June, 2013. Dedicated to David Kenning paying tribute to his great achievements in nucleate boiling science.

ABSTRACT

Prediction of heat transfer in the evaporator of a refrigeration unit should be as accurate as possible for the successful operation of the whole appliance. The predictive methods used at present are empirical or semi-empirical, particularly for the heat transfer conditions relevant in practice, because theoretically consistent calculation of the heat transfer coefficient in nucleate boiling is not yet possible. One of these which is included in the VDI Heat Atlas and has been updated recently, is presented in the first main part below and is compared with experimental data for 55 fluids. In the second, eight more prediction methods from the literature are tested using the same experimental database, and the deviations between measurement and calculation are discussed in detail together with the different results calculated with the various methods.

KEYWORDS:

Heat transfer; nucleate pool boiling; prediction method; thermophysical properties; experimental databank.

NOMENCLATURE:

A, m	factor ($kW\ m^{-2}K^{-1}$) or exponent of Eq(6)
C_w	factor for material of heated wall
c_ℓ	heat capacity of saturated liquid ($J\ kg^{-1}K^{-1}$)
D	diameter of heated tube (m)
d_b	bubble departure diameter (m)
g	gravitational acceleration ($m\ s^{-2}$)
$\Delta h_{\ell g}$	enthalpy of vaporization ($J\ kg^{-1}$)
M	molar mass ($kg\ kmol^{-1}$)
p	pressure (bar or $N\ m^{-2}$)
p^*	$= p/p_c$, reduced pressure
P_f	$= (dp/dT)_{VPC}/\sigma$ characteristic boiling parameter of the fluid $(K \cdot \mu m)^{-1}$
q	heat flux ($W\ m^{-2}$ or $kW\ m^{-2}$)
R	individual gas constant ($J\ kg^{-1}K^{-1}$)
R_a	arithm. mean roughness height (ISO4287)(μm)
$R_{p,old}$	$= R_a/0.4$ “Glättungstiefe“ (DIN4762)(μm)
T	temperature (K or $°C$)
T_{sN}	temp. at normal boiling point
ΔT	superheat, surface of heated wall (K)

Greek:

α	heat transfer coefficient ($W\ m^{-2}K^{-1}$ or $kW\ m^{-2}K^{-1}$)
α_0	$= \alpha$ for a copper tube at $q_0 = 20\ kWm^{-2}$, $p_0^* = 0.1$, $R_{a0} = 0.4\mu m$
$\alpha_{0.1}$	$= \alpha_0$ for $R_a = R_{a,exp}$
β	contact angle (deg)
ρ_ℓ, ρ_g	density, saturated liquid or vapour ($kg\ m^{-3}$)
λ_ℓ	thermal conductivity of saturated liquid ($W\ m^{-1}K^{-1}$)
η_ℓ, ν_ℓ	dynamic or kinematic viscosity of saturated liquid ($Pa \cdot s$ or m^2s^{-1})
σ	surface tension of saturated liquid ($N\ m^{-1}$)

Subscripts:

c	critical state	ref	reference value
Cu	copper	s	saturated state
f	fluid	VPC	vapour pressure curve
0	normalizing value	w	heated wall

1. INTRODUCTION

Prediction of heat transfer existing e.g. on the flooded bundle of horizontal tubes in large evaporators of refrigeration units should be as accurate as possible for the successful operation of the entire plant. The predictive methods used at present are empirical or semi-empirical, particularly for the heat transfer conditions relevant in practice, because theoretically consistent calculation of the heat transfer coefficient α in nucleate boiling is not yet possible (see e.g. the reviews in Stephan, Fuchs (2009), Kenning et al. (2009), Dhir (2006), Kenning (1999), Gorenflo et al., 1998). Most of the methods have been established as power laws in the past, containing separate factors for the main parameters that are of influence in nucleate boiling heat transfer.

One of these is included in the VDI Heat Atlas since 1984 (Gorenflo, 1984) and has been updated recently. It will be presented in the first main part of the paper and compared with experimental data for 55 fluids. In the second, eight more prediction methods from the literature will be tested using the same experimental database, and the deviations between measurement and calculation will be discussed in detail together with the different results calculated with the various methods.

2. UPDATE OF THE HEAT ATLAS PREDICTION METHOD

2.1 Outline of the Method

In the Heat Atlas prediction method (Gorenflo, Kenning, 2010; Gorenflo, 2013), the main groups of variables that are of influence on the heat transfer coefficient α are considered in separate factors to establish a reduced heat transfer coefficient α/α_{ref} of the form

$$\alpha/\alpha_{ref} = F_q(q/q_0)\cdot F_{p^*}(p^*/p^*_0)\cdot F_f(P_{f0}/P_{f,ref})\cdot F_w \qquad (1).$$

The reference heat transfer coefficient α_{ref} is a *constant* reference value for *all* fluids, independent of the influences on the right hand side of Eq(1). The functions F are *independent nondimensional* functions,

- F_q and F_{p^*} for the relative increases of the heat transfer coefficient α with rising heat flux q and reduced pressure $p^* = p/p_c$ (p_c = pressure in the critical state),
- F_f for the influence of the thermophysical properties of the fluid at the reference pressure p^*_0, and
- F_w for the influences of surface roughness and material of the heating wall.

The reference values $q_0 = 20\text{kW/m}^2$ and $p^*_0 = 0.1$ represent typical mid-range conditions of nucleate boiling in industrial applications. The reference state for the heating wall is a horizontal copper cylinder with an intermediate value $R_{a0} = 0.4\mu\text{m}$ of the arithmetic mean roughness height (ISO 4287), which lies within the common range for heater surfaces used in practice. Finally, $P_{f,ref}$ is a reference value (also in mid-range) for the characteristic combination P_f of thermophysical properties of the fluid at the reference pressure $p^*_0 = 0.1$, as will be shown later. The concept is demonstrated in Fig.1 in the well-known log/log-representation of α over q for i-Butane boiling on a horizontal copper tube at different reduced pressures p*: F_f is providing the value α_0 for i-Butane at reference conditions p^*_0, q_0 and R_{a0}, and α_2 can be calculated for heat fluxes and reduced pressures other than in the reference state, using F_{p^*} and F_q from Fig.2.

{Here Fig.1. (It may be reduced in size to one column = width of 84mm.)}

Fig.1: Concept of the calculation method shown for i-Butane boiling on a copper tube

The steep slopes of the straight lines – corresponding to the exponent n of the heat flux in Eq(2) – show the strong increase of α with q at p* = const. A similar increase is existing for α with p* at q = const, e.g. $q = q_0$, dashed straight line, both well-known for nucleate boiling heat transfer.

Nucleate boiling is ending in free convection without bubble formation at small heat fluxes and reduced pressures (dot-dashed straight line), and in the maximum heat flux q_{crit} (burnout) at high heat fluxes (dashed curve in Fig.1). The latter has been calculated by the prediction method for q_{crit} updated in 2013 for the 11th ed. of the Heat Atlas. For q-values close to q_{crit} or if very high α-values result from Eq(2) (hatched zone), it is recommended to check the calculated data by experiment. Nevertheless, the straight interpolation lines

continue to be valid up to very close to q_{crit} in recent experiments, see Kang et al. (2009) and Gorenflo et al. (2010).

In the following, the updates for the influences of q, p* and the properties of the fluid will be discussed, and for some non-updated influences, new experimental evidence will be shown.

2.2 Update of the influences of heat flux and pressure for single tubes

The relative increase of α with q – symbolized by F_q in Eq(1) – is represented by

$$F_q = \alpha/\alpha(q=q_0) = (q/q_0)^{n(p^*)} \qquad (2),$$

where n(p*) has been updated to

$$n(p^*) = 0.95 - 0.3\, p^{*0.3} \qquad (2a),$$

and the update of the relative increase of α with p* is given by

$$F_{p^*} = \alpha/\alpha(p^*=p^*_0) = 0.7\, p^{*0.2} + 4\, p^* + [1.4\, p^*/(1 - p^*)] \qquad (3),$$

with all other parameters in Eq(1) remaining constant. For water, relationships that differ somewhat from Eqs(2a) and (3) were established in 1984 for the Heat Atlas and should continue to be applied because no new experimental results have been found to support an update.

For the update, own new experiments with 23 fluids (8 partly fluorinated refrigerants, 7 hydrocarbons, 5 alcohols, and 3 fluids from other groups) and a literature review – containing also other experimental data of these and 5 additional hydrocarbons – have been used (Kotthoff, 2014). The review for hydrocarbons has already been published in 2008 (Kotthoff, Gorenflo, 2008).

In Fig.2, the α(q)- and α(p*)-dependencies for the ***own experiments*** are shown in terms of the exponent n(p*) in the upper diagram, and of the ratio $\alpha/\alpha_{0.1}$ in the lower, where $\alpha_{0.1}=\alpha$ at the reference pressure $p^*_0=0.1$ and the reference heat flux q_0, but $R_a=R_{a,exp}\neq R_{a0}$. The heater was a horizontal copper tube of 8mm O.D. with twice sandblasted surface (fine then coarser corundum grain). All fluids were planned to be investigated with the same heater (tube #1), but it was damaged after 8 fluids, so another with identical design had to be used (tube #2, see symbols with dash in Fig.2) for the remaining 15 fluids, or 16, resp., because the tests for R134a were repeated with the 2nd heater. The experimental equipment and procedure that had been developed earlier was explained somewhere else again recently (Gorenflo et al., 2010).

{Here Fig.2 (width should not be reduced below about 130mm because of the many different data given)}

Fig.2: Pressure dependence of n and relative pressure dependence of α for the own new experiments with 23 fluids and comparison with the correlations of the Heat Atlas

As follows from both diagrams in Fig.2, all the data lie within the same limits of experimental scatter (shaded areas), *without systematic deviations between the different groups of fluids.* The same had been found earlier for the data set used in 1984 for the 4th German edition of the Heat Atlas, up to the 10th ed., 2006, see Gorenflo (1984). The bars added to the symbols for n indicate the maximum scatter, if n is fitted only to high or low q-values, respectively.

The new experimental α(p*)- and α(q)-dependencies are significantly more pronounced than according to the former calculation method – the latter visible from higher exponents n – as can be seen from the comparison of the symbols with the dashed curves. A similar trend had already been exhibited by experimental data sets in Gorenflo et al. (1990, 1991).

{Here Fig.3 (please, use the entire height of a page and don't put Fig.3 within the text of the next section)}

Fig.3: Pressure dependence of n and α for the new experiments of the literature review and comparison with the Heat Atlas calculation method. Top: Hydrocarbons (together with the overall scatter of the former

experimental Heat Atlas database for organic fluids). Bottom: Refrigerants, alcohols and 3 fluids from other groups

In Fig.3, the results of the ***literature review*** have been added for the three groups of fluids (hydrocarbons, refrigerants, and alcohols & others). The new trends of the review correspond to Fig.2, while the overall scatter has markedly increased due to the greater variation in the experimental conditions existing at the various investigations. The updated Eqs(2) & (3) do not reflect the entire differences between the new data and the former correlations because the former database was also considered in the update. For a significantly more detailed discussion of the 12 hydrocarbons included in the review, see Kotthoff, Gorenflo (2008).

2.3 Updated influence of thermophysical properties

The influence of the thermophysical properties of the fluid on α has been separated more or less arbitrarily in two parts, **one** that is represented by F_f in Eq(1) and is caused by the variation of the properties of *different fluids* at the *constant reduced* pressure p^*_0 , and **another** which is related to the variation of the properties of *the same fluid* with pressure and is represented within F_{p^*} or Eq(3), respectively. This one is a consequence of the properties varying with *temperature* along the vapour pressure curve, and it is a combined pressure-temperature effect as can be seen from Eq(5). At the end of the paper, it will be discussed more in detail.

But before, the part in F_f at p^*_0 = const will be analyzed. It can be modeled by means of the fluid-specific parameter P_f which is the ratio of slope of the vapour pressure curve (VPC) and surface tension σ, both at the reduced reference pressure $p^*_0 = 0.1$,

$$P_f = (dp/dT)_{VPC} / \sigma \qquad (4).$$

P_f follows from the simplified Thomson Equation for the increment Δp of pressure necessary within a spherical bubble nucleus with radius r, if Δp is produced by the superheat ΔT of the liquid in the boundary layer around a heated tube at constant pressure p^*_0 ,

$$\Delta p = 2\,\sigma / r \approx (dp/dT)\,\Delta T \qquad (5).$$

P_f was used first in Kotthoff, Gorenflo (2005). It results from former plots employing it in its reciprocal form (Bier, Lambert (1990); Gorenflo et al., 1991) for modeling the superheat ΔT, and from considerations to find those properties of the fluid that are important for nucleate boiling (Bier et al., 1973, 1977, Gorenflo, 1977). The latter was summarized more recently in Gorenflo et al. (2004).

In Fig.4, the absolute values $\alpha_{0.1}$ at $q_0 = 20 kW/m^2$, $p^*_0 = 0.1$, and $R_a = R_{a,exp}$ for the 23 fluids of the **own experiments** used as reference values in Fig.2 have been plotted over the fluid parameter P_f in double logarithmic scales. As can be seen from the upper two diagrams, the results for both tubes can be interpolated fairly well by straight lines, with maximum deviations from the measurements for CO_2 & n-Pentane (+12.6% or -9.6%) in case of tube # 2, and for R125 & R152a (-10.2% or +8.8%) in case of tube # 1.

{Here Fig.4 (width should not be reduced below about 120mm because of the many different data given)}

Fig.4: $\alpha_{0.1}(P_f)$-representation for the own new experiments with 23 fluids boiling on the two copper tubes # 1& 2. Top: Separate diagrams for tube # 1 or # 2. Bottom: Data for both tubes compared with Eq(6) adapted to $R_{a,\,exp}$ (dashed lines) and with earlier data for 3 of the fluids boiling on a fine sandblasted 25mm-tube (#3, small symbols; from Danger, 2004)

For the updates of the Heat Atlas (Gorenflo, Kenning, 2010; Gorenflo, 2013), the sources in the data banks for the two thermophysical properties in Eq(4) have been revised. As a consequence, the values of P_f from Kotthoff, Gorenflo (2005) were modified significantly for 5 fluids, see the horizontal lines pointing to symbols in the upper two diagrams of Fig.4. Thus, the deviations of the interpolation lines from the α-measurements have been reduced in 4 cases. In addition, 4 of the new P_f-values better fit the sequence of fluids within the group they belong to, because originally: Cyclohexane was closer to Heptane than Hexane, n-Propanol closer to 2-Butanol than 2-Propanol, 2-Propanol closer to Ethanol than n-Propanol. In addition, the value for R143a appeared beyond R125, instead of lying between R152a and 134a as follows for the 3

refrigerants from the number of F-atoms in the molecules with the same structure: All of them are Ethane derivatives with asymmetrical distribution of the F-atoms among the two C-atoms. For the sequence in Fig.4 to be "correct", P_f should be higher or lower by merely 1% for R134a or 143a, respectively.

Obviously, the poor accuracy of the data for surface tension is responsible for the modifications, with uncertainties given in the Heat Atlas data bank for the fluids of Fig.4 between ±2% and ±10% (Span, 2010). As a consequence, the deviations of the experimental data from the interpolation lines may result from both, small individual effects in heat transfer for certain fluids or uncertainties of the properties in P_f. Calculating P_f for Ethanol from the data in Refprop 9.0 (Lemmon et al., 2010) would result in $1.89(\mu mK)^{-1}$ – i.e. P_f for Ethanol would lie even beyond the value for Methanol.

The direct comparison of the data for the two tubes in the lowest diagram of Fig.4 reveals that the slopes of the interpolation lines for tube #1 & 2 are exactly the same, but the interpolated $\alpha_{0.1}$-values differ for 14%. The difference is almost the same as in the α-values measured for R134a with both tubes: 15%, see the diamonds with or without dash. It demonstrates that the shift of the two upper full interpolation lines is an effect of the different heaters, and that a *general relative influence* of the properties of the fluid exists with an $\alpha(P_f)$-dependency that can be represented by the power law of Eq(6), $\alpha = A\ P_f^m$, as had been postulated in (Kotthoff, Gorenflo, 2005).

Further support comes from Propane and 2-Propanol which have been measured now with *different* tubes #1 & 2, see #21 & 13 in the upper diagrams of Fig.4. Earlier, both fluids had been investigated together with R134a (Danger, 2004) using the *same* copper tube for all of the 3 fluids (tube #3, D = 25mm and fine sandblasted surface, lowest diagram of Fig.4). And also for this heater, the power law of Eq(6) is valid for the relative influence of the fluid properties, with only slightly smaller slope which, however, remains well within the range of slopes that could be derived from the experimental scatter for the other two tubes.

Although the influence of the heater on α will not be analyzed before the next section 2.4, the roughness term F_R of Eq(7) is used for Fig.5 already now, because discussion of the **new literature review** requires to reduce the heat transfer coefficients for copper heaters with different $R_{a,exp}$ from the literature (including those of Fig.4) to the reference value R_{a0} = 0.4µm. The data of Fig.4 and the new literature review (small symbols) and the former experimental database of the Heat Atlas (up to 7th ed.,1994, big open symbols) have been represented in Fig.5 together with the update of the latter that resulted in the shaded big symbols. The experimental data entered the update with different weight depending on number of data and information on experimental details available.

{Here Fig.5 (width should not be reduced below about 120mm because of the many different data given)}

Fig.5: Update of the former experimental database for α_0 (big open symbols) in the Heat Atlas by new experiments (small symbols) and comparison with the updated database (shaded big symbols) and the $\alpha_0(P_f)$-correlation

The new data include 93 sources for 28 fluids, for 63% of the sources the diameter of the heating copper tube was D = 8mm and for the rest, the D-range was from 15 to 25mm (with one exception). Examples for the influence of diameter on α are given in Kotthoff, Gorenflo (2012) and Kotthoff (2014) – see also Methanol and 2-Propanol in Fig.5. The experimental evidence with a maximum in α for D between 30 and 50mm, however, is not yet clear enough to include it in the calculation method.

In 2005 already, the power law of α with P_f had been fitted to the experimental database existing in the 9th ed. of the Heat Atlas at that time, producing the preliminary values A = 3.6kW/m²K and m = 0.6 (Kotthoff, Gorenflo, 2005). In the new fit, only A has been modified slightly to 3.58kW/m²K. The final, *nondimensional* form of the factor F_f in Eq(1) was achieved by interpreting A as reference value of a fictitious fluid with the intermediate parameter $P_{f,ref}$ = 1(µmK)$^{-1}$ and with the mean experimental $\alpha_0(P_f)$-relation of Fig.5 and Eq(6),

$$F_f = \alpha_0/\alpha_{ref} = [(P_f/P_{f,ref})^{0.6}]_{p^*0=0.1}\ ,\quad with\ \ \alpha_{ref} = 3.58\ kW/m^2K,\ \ P_{f,ref} = 1\ (\mu m\ K)^{-1} \qquad (6).$$

As can be seen from Fig.5, the **updated** $\alpha_{0,exp}$-values (shaded big symbols) of the Heat Atlas data bank are well represented by Eq(6). Comparison with the database before the update (open big symbols) reveals that

distances from the calculated line diminished by the update for most of the fluids – for some drastically, e.g. i-Pentane, Acetone, 2-Propanol. There is one severe deviation, however, for an updated fluid, that occurs in case of Ethene. The reason might be that insufficient purity of the fluid used or an experimental error are involved in the Ethene-data, because α_0 is much too small if compared with Ethane and with the α_0-difference for Propane & Propene in the upper diagram of Fig.5. A more detailed discussion of the problem can be found in Gorenflo et al. (2012) and Kotthoff (2014). All 28 updated values of Fig.5 are also shown in the upper two diagrams of Fig.6, and except for the one big deviation, the *maximum* scatter remains within ±10%.

{Here Fig.6 (please use the entire width of a page because of the many different data given)}

Fig.6: Comparison of the $\alpha_0(P_f)$-correlation with the new experimental database of the Heat Atlas.
Upper two diagrams: updated fluids; lower two diagrams: non-updated fluids and H_2O, NH_3.

In the lower two diagrams of Fig.6, also the $\alpha_{0,exp}$-values for the **non-updated** fluids of the Heat Atlas data bank are compared with Eq(6), together with water and ammonia. For these two fluids, only a few new data exist that do not require an update, see also the detailed discussion for NH_3 in Kotthoff, Gorenflo (2008). The non-updated fluids extend the range for P_f from $0.69 < P_f < 3.15$ for the updated fluids to $0.53 < P_f < 20.5$ $(\mu m\ K)^{-1}$, i.e. from a factor of about 4.5 to about 40. For Helium which is also included in the experimental data bank, Eq(6) cannot be applied because nucleate boiling ends for this fluid at heat fluxes well below the reference value $q_0 = 20 kW/m^2$.

As can be seen from the lower diagrams, the experimental data are well represented also for the extended range, the maximum scatter, however, has increased from ±10% for the updated fluids to ±20% for the non-updated, cf. the dashed straight lines in Fig.6. The numerical values in the two Δα-diagrams differ somewhat because being related to $\alpha_{0,exp}$ instead of $\alpha_{0,calc}$ as for the dashed lines. Among the deviations >10%, there are significantly more fluids with $\alpha_{0,exp} < \alpha_{0,calc}$ see 11 fluids near lowest dashed line for -20%. It is likely that this is an effect of the former measuring techniques not being at the level of today, because in 1984, also experimental data had been included in the data bank that originated from 20 to 30 years behind. Together with the comparatively high α_0-values, this may result in deviations *to the lower*.

By the same diagrams, it is also proved that the "fictitious, intermediate" fluid with $P_{f,ref} = 1(\mu mK)^{-1}$ in fact is situated close to the (logarithmic) center of the P_f-range for the fluids important in industrial application, if the cryogens beyond CF_4 (with $T_s = -106^oC$ at $p^*_0 = 0.1$) are not taken into account. On the other hand, also the "real" fluid i-Butane with $P_f = 1.062\ P_{f,ref}$ could have been taken as reference fluid because its mean experimental α_0-value is almost identical to $\alpha_{0,calc}$ (3.70 instead of $3.71 kW/m^2K$, see the upper two diagrams).

A first successful application of the prediction method was possible in the PhD thesis of Buljina (2010) when α-values for the two pure components were needed to calculate the deterioration of nucleate boiling heat transfer for the very wide-boiling binary system n-Pentane/Hexadecane ($C_{16}H_{34}$). The difference of the normal boiling points of the components for this system amounts to $\Delta T_{sN} = 250K$. For experiments with the latter pure component saturation temperatures being too high ($T_{sN} = 286^oC$) because of thermal dissociation, $\alpha_0 = 2.28 kW/m^2K$ was determined from Eq(6) for $P_f = 0.47(\mu mK)^{-1}$ of this fluid (closed diamond in the lowest diagram of Fig.6). α-values for q and p* other than in the reference state were determined using the calculated α_0-value and Eqs(2) & (3). Thus, the calculation method was applied *without any experimental* information on nucleate boiling heat transfer for the higher boiling component of this binary system.

The diagram also indicates that the α_0-values for the saturated paraffinic hydrocarbons with 8 to 15 C-atoms will lie within the small range between $P_f = 0.7(\mu mK)^{-1}$ for C_7H_{16} and $0.47(\mu mK)^{-1}$ for $C_{16}H_{34}$ which appears on the straight line close to the lower left end of the lowest diagram in Fig.6. Besides that, the 8 values could be estimated with errors <10% *even without calculating* P_f, only by using the systematic decrease of the updated α_0-values within $C_{2,4,6}$ or $C_{3,5,7}$, resp., as can be verified quite easily from Fig.5 or from the first column on the left of Table 3 in Section 3.

Deviations significantly beyond +20% occur only for the highly associating fluids H_2O & NH_3 and for i-Butanol. The latter has been put in brackets together with n-Butanol in Fig.6 because both of their $\alpha_{0,exp}$-values should be close to 2-Butanol instead of differing for more than 40%. This follows from comparing not

only with their updated isomere 2-Butanol, with n & 2-Propanol, but also with the experimental $\alpha_{0,exp}$-data of the other 6 updated isomeres in Fig.6 and Table 3 of Section 3 (n & 2-Propanol, n,i-Butane, n,i-Pentane).

{Here Fig.7 (same width as Fig.5 and please, don't insert the figure in the text of the next section 2.4)}

Fig.7: $\alpha_0(P_f)$-dependence for discussion of new measurements with n-Butanol and the new refrigerant R1234yf

In Fig.7, n & i-Butanol have been added to the updated fluids of Fig.5 for direct comparison of the 9 isomeres cited above. In addition, two new experimental values for n-Butanol are shown (small symbols) that result from measurements with a Cu-tube with D = 4mm and two surfaces with different roughness (emeried: R_a = 0.55µm or rough sandblasted: R_a = 1.91µm; Gremer, 2001). Adapting to R_{a0} = 0.4µm by Eq.(7) and to D = 8mm by taking into account the influence of diameter as reported in (Kotthoff, 2014), ends up in the two small symbols at 3.20 or 3.43kW/m^{2}K, slightly below or above the value calculated for n-Butanol from Eq(6). A similar correction towards the calculated value can be expected from new measurements with i-Butanol. (More details about deviations from Eq(6) for certain fluids are given in Gorenflo et al., 2012 and Kotthoff, 2014.)

The new measurements for n-Butanol with the small tube did not enter the update because the method to consider the influence of diameter on α is not yet well established. Recent measurements with the new refrigerant R1234yf (H_2C=CF.CF_3) neither entered the update, but for the different reason that only *one* source was found in literature for this partly fluorinated Propene-derivative (Park, Jung, 2010). Its experimental α_0-value is markedly smaller than $\alpha_{0,calc}$ from Eq(6) (3.00 or 3.87kW/m^{2}K) as can be seen from comparing the closed small symbol on the left of the Propane-derivative R227ea with the full straight line in Fig.7, bottom. A similar systematic shift to the lower is found for all the measurements of the Korean group of Jung et al. (see all closed small symbols in Fig.7), so it is likely that new measurements of another group of researchers will reduce the difference to Eq(6) also for this fluid.

Having in mind the huge scatter of experimental data for the same fluid in case of the very often investigated refrigerant R134a or hydrocarbon Propane, in the lower or upper diagram of Fig.7, respectively, this highlights again how important it is to have a set of experimental data originating from the *same* equipment and experimental procedure for a great number of fluids as in case of Fig.4, for finding relationships as Eq(6).

On the other hand, also the entire data set originating from 3 teams of the Korean group mentioned above exhibits the same relative increase of α_0 with P_f as Eq(6). This is seen from the closed small symbols in Fig.7 and their 3 dashed straight interpolation lines for 4 hydrocarbons (Jung et al., 2004) and 3 or 2 refrigerants (Jung et al., 2003) or (Park, Jung, 2007, 2010), wich are running exactly parallel to the full lines for Eq(6). (For further results see also the discussion of Figs.9 & 12, and correlation # 3 of this group in Table 1.)

2.4 Non-updated influences

Besides the updated parts discussed in 2.2 and 2.3, other parts have been updated in the most recent edition of the Heat Atlas (11th ed., Gorenflo, 2013), but will not be discussed here (prediction of the maximum heat flux q_{crit} (burnout) of nucleate boiling or minimum heat flux q_{min} of film boiling (Leidenfrost Point) and of heat transfer with film boiling). There are also various parts *without update*, for which new experimental evidence has been introduced in the new edition of the Heat Atlas, e.g. for bundles of horizontal tubes, heating surfaces with fins, boiling of mixtures, or for the influence F_w of roughness and material of the heater.

Although there are not enough new experimental results for updating the **influence F_w of the heater**, it will be discussed here because it is one of the important factors in Eq(1) and has already been used above for the review. It reads

$$F_w = F_R\, F_M = (R_a / R_{a0})^{2/15}\, [(\lambda\rho c)_w / (\lambda\rho c)_{Cu}]^{1/4} \qquad (7),$$

where the first part F_R was developed by Stephan (1963) for another roughness parameter and the second (F_M) was introduced in the calculation method for the 7th ed. of the Heat Atlas in 1994 (the latter will not be discussed further because only heaters with copper as wall material are regarded here). Originally,

"Glättungstiefe" R_p of the former German standard DIN 4762 was used by Stephan because it could be related to the volume of vapour within the roughness cavities of the heating surface. This relation cannot be established for any of the parameters in the new standard ISO 4287. Schömann, however, showed in 1994 that a formal relationship

$$R_a = 0.4\, R_{p,old} \qquad (8)$$

exists between R_a of the new standard and the former parameter $R_{p,old}$ over a large range of R_a-values for metal surfaces finished in different ways. The abbreviation $R_{p,old}$ is used here and throughout the paper for "Glättungstiefe" in order to avoid confusion with the parameter R_p which is defined in an entirely different way in the new standard.

Subsequently, modifications of the Stephan Equation have been developed which are incorporated in three of the prediction methods (besides the Heat Atlas method) listed in Table 1: Two are containing a slight influence of p* (#1 & # 4) and one a slightly more pronounced increase of α with R_a (but without influence of p*: #2). In all of them, the same drawback is included as in Eq(7) that only *one, average* value of *one* roughness parameter is used for the whole heating surface to model the influences of the shape (re-entrant or not) and size of the roughness cavities that are activated as nucleation sites. According to Eq(5), smaller cavities will be activated with increasing reduced pressure at constant q because of decreasing σ, or with increasing heat flux at constant p*, because of increasing ΔT.

{Here Fig.8 (width should not be reduced below about 120mm because of the many different data given)}

Fig.8: Relative differences Δα for copper tubes with different surface roughness:
Comparison of measurements (partly closed symbols and full lines) with calculated data for 4 of the prediction methods in Table 1 (open symbols and dot-dashed lines)

In Fig.8, the 4 $\alpha(R_a)$-correlations are compared with α_{exp} using the relative difference in α for two couples of heaters with the same diameters, but different surface roughness produced by different (fine sandblasted or emeried, upper diagram) or smilar treatment (sandblasted with fine grain or fine then coarse grain, lower diagram). The following can be seen from the comparison:

- The relative differences in α increase with decreasing heat flux at constant p* – being highest for small q-values near free convection without bubble formation.
- The influence of p* (at q = const) contains a clear maximum near 10% of the critical pressure, which is becoming less pronounced for high heat fluxes.
- The overall effect is significantly stronger for the two surfaces with different treatment (upper diagram) – despite the smaller relative differences in the R_a-values.

None of the correlations does not contain neither the influence of q nor the maximum in the influence of p*. Nevertheless, for high heat fluxes q > 20kW/m^2, where the α-differences for about factor 2 in R_a decrease to 20% or less, also the differences between measured and calculated α-values become small. Thus for the sake of simplicity, it was kept to the term F_R in Eq(7) until a calculation method for the influence of roughness on α will be available where at least the size distribution of a suitable roughness parameter has been included. This had already been recommended by Stephan (1963), and it is also following from many investigations ever since cited e.g. in Luke (1996) & Kotthoff (2014).

A modification of this kind would allow to predict even those results in the literature where the $\alpha(R_a)$-relationship of F_R turns upside down, i.e. α decreasing for increasing R_a. The effect occurs particularly for surfaces with high roughness as was shown by systematic measurements in the wide q, p*-ranges of Fig.8 already in 1979 for two copper plates with different surface structures produced by turning, but each of the structures being uniform. One was very smooth with R_a = 0.2, and the other ended up very rough on purpose, but with parallel grooves of regular shape and R_a = 2.2µm (Salem, 1979).

All in all, the above discussion clearly demonstrates that modeling the influence F_w of the heating wall is by far the weakest point in the prediction methods and that representation of this influence in the methods should be improved with high priority. At the end of the first main part of the paper, two new sets of

experimental data are presented that confirm the (non-updated) parts of the Heat Atlas prediction method for the influence of fins on horizontal heaters (Fig.9) and for bundles of horizontal tubes (Fig.10).

At low to intermediate heat fluxes and reduced pressures, **heaters with fins** (integral, trapezoid-shaped or "K-shaped") transfer heat more efficiently than heaters with plain surfaces. This also follows from the new example in Fig.9 for measurements of Park & Jung (2010) with small finned or plain Cu-plates (that could be used for cooling of electronic devices), see the lower two interpolation lines for symbols with or without dashes. The higher heat transfer coefficients for finned surfaces are caused by the rough crests of fins that originate from the production process of internal fins, and by additional convection of bubbles sliding along the flanks of the fins.

{Here Fig.9 (width should not be reduced below about 100mm because of the many different data given)}

Fig.9: $\alpha(q)$-dependency for R134a and the new refrigerant R1234yf boiling on flat plain or finned copper plates (from Park, Jung, 2010, extended)

Both effects increase heat transfer at low heat fluxes q more than at high, therefore the *relative* increase of α with q is less pronounced for finned surfaces. The relative increase of α with p* is also weaker because convective heat transfer is nearly independent of pressure or even *decreasing* with p* because bubbles and the entire vapour volume produced at q = const become smaller at higher p*. As a consequence, the increase of F_q in Eq(1) with q and p* will be weaker (or the exponent n be smaller, resp.) and also F_{p*} will increase less with p* than for plain tubes.

Without explaining this part of the calculation method more in detail, it postulates: (a) Heat transfer coefficients should be the same for plain and finned surfaces at 100kW/m^2. This is exactly existing for the measurements, if the data for the finned plate are somewhat extrapolated, see the bold vertical dashed line in Fig.9. (b) For finned surfaces, the experimental n_f of Eq(2) should be smaller than n for plain ones, according to $n_f = n - 0.1h/t_\ell$, with h – height of the fins and t_ℓ - gap width between the fins. Also this is verified by the experiments within experimental scatter.

The heat transfer coefficients are the same for both refrigerants at T_s = 7°C, see circles for R1234yf or triangles for R134a because both were investigated by the same group, and because the slightly lower α_0-value of R1234yf in Fig.7 is compensated by the (slightly) higher reduced pressure at this temperature than with R134a (p* = 0.122 instead of 0.092).

{Here Fig.10 (width should not be reduced below about 110mm and figure not be put in next section 3!)}

Fig.10: $\alpha(q)$-dependency for R134a (upper diagram) and the new refrigerant R236fa (lower diagram) boiling on a bundle of horizontal copper tubes at 4 saturation temperatures between 5 and 20°C.

Big symbols and dashed straight interpolation lines: experimental data from (van Royen et al., 2012).

Small symbols and full curves or straight lines: calculated data for a bundle or single tubes, respectively, from Heat Atlas prediction method.

In Fig.10, recent measurements of the group of John Thome (van Royen et al., 2012) with R134a and the new refrigerant R236fa boiling on a **bundle of horizontal plain copper tubes** (D = 18.95mm; T_s = 5 to 20°C; q = 5 to 30kW/m^2) are compared with calculated data using the Heat Atlas prediction method.

The calculation procedure is outlined in the upper diagram: The average heat transfer coefficient α_{bundle} is separated in a purely formal way into α_u for the lowest row of tubes and the relative improvement (α_{bundle}/α_u) within the bundle. α_u is calculated by additional superposition of the heat transfer coefficients $\alpha_{one,nb}$ for nucleate boiling and $\alpha_{one,conv}$ for free convection without bubbles, both for a single tube. The range for the factor f is $0.5 \leq f \leq 1$. f = 1 has been chosen for the marked convection produced by the narrow pitch of 1.173D for the staggered, equilateral triangle layout used in the experiments. For the relative improvement within the bundle, a *dimensional* function of the heat flux q in kW/m^2 is used as derived from experimental data in the literature (cf. e.g. Gorenflo, 1984).

For the comparatively big diameter of the tubes, the turbulent variant of Nu = f(Ra) is used (given in Fig.10) to calculate $\alpha_{one,conv}$ for both fluids, and $\alpha_{one,nb}$ is calculated as demonstrated in Fig.1, also for both fluids. For the Propane-derivative R236fa, however, it should be mentioned that calculation is *entirely predictive* because not any experimental data entered the calculation procedure for this fluid and single tubes. It starts with Eq(6) to get $\alpha_{0,calc} = 3.76 kW/m^2K$ from $P_f = 1.087(\mu mK)^{-1}$ at q_0, p^*_0 and R_{a0}. Then Eq(7) has been used considering that $R_{a,exp}$ will be about 0.6µm. Finally, Eqs(2 & 3) have been used for other values of q and p*.

In the paper of van Royen et al. (2012), the only roughness data given is 2.30µm as average value for the *new* parameter R_p. The new parameter, however, is defined in an entirely different way than the former parameter $R_{p,old}$, e.g. incorporated in the correlation of Stephan (1963) see the above discussion of Eqs(7 & 8), and also in those of Nishikawa et al. (1982) and Cooper (1984), see # 4 & 1 in Table 1. It is known from own measurements that R_a will amount to about 0.6µm for conventional copper surfaces, if $R_{p,new} = 2.30\mu m$ has been measured as in the experiments of Fig.10. Then the former parameter will result in $R_{p,old} = 1.5\mu m$ according to Eq(8).

It can be seen from both diagrams: (a) The 3 *calculated* full lines for 10/15/20°C are more or less *equidistant* for single tubes or the bundle, but: (b) The distances for the bundle are somewhat smaller because of the convective contribution to heat transfer, which is approximately independent of pressure. (c) The lines for the bundle are curved because the relative influence of convection increases towards smaller heat fluxes, and finally: (d) This latter effect is more pronounced for the lower reduced pressures with R236fa (see the bigger distance between the straight lines and the curves for this fluid at $q = 2 kW/m^2$) because $\alpha_{one,nb}$ is smaller in the pertaining pressure range and Nu = f(Ra) is nearly independent of pressure.

Comparison between dashed straight lines interpolating the experimental data for the bundle and calculated full curves reveals ***for both fluids*** (a) that $\alpha_{calc} < \alpha_{exp}$ holds throughout the q- & p*-ranges of the experiments, (b) that the difference between measured and calculated values is smallest at 10°C and increases systematically for the two higher temperatures (or pressures), and (c) that the experimental peculiarity for 5°C, with α-values being approximately the same as for 15°C, does not exist in the calculation.

A more detailed investigation reveals ***for R134a*** in the upper diagram that the calculated values lie within the experimental scatter for 10°C, deviate to the lower for less than 10% at 15°C, and deviation increases to -20 or -30% at 20°C for the highest or lowest experimental q-value, respectively. For **R236fa** in the lower diagram, the deviations of the calculated values to the lower are found to be less than 10 or 20% at 10 or 15°C, respectively, and at 20°C, the deviations are approximately the same as for R134a.

It is remarkable that in the case of R134a (upper diagram), α_{exp} for the bundle is almost independent of pressure between 5 and 15°C in the restricted q-range of the measurements at 20°C. On the other hand, however, the relative increase from 15 to 20°C is about twice or three times the one following from the p*-dependence of Eq(3) for single tubes at the highest or lowest experimental q-value at 20°C, respectively. Having in mind the discussion for Fig.9 about convection caused by bubbles, and that the relative increase of α with p* as predicted by Eq(3) is most pronounced in the pertaining p*-range of $0.12 < p^* < 0.14$, if compared with all the other correlations in the lower diagrams of Fig.11, the effect is likely to be caused by special features during the experiments.

Finally, the following should be mentioned: (a) In the above comparison, the *own* interpolation lines of Fig.10 have been used which differ slightly from the α(q)-equations given in the paper of van Royen et al. (2012) for the 4 pressures. (b) The experimental α(q,p*)-dependency for the other fluid is not explicitly given in the paper as for R134a, that is why the above comparison has been restricted to R134a. Instead: (c) The α(q)-equations of the paper for the interpolation lines have been used for R236fa in the lower diagram of Fig.10 (dashed straight lines) and the experimental limits α_{max} or α_{min} have been extracted from a diagram of α_{calc} over α_{exp} in the paper, which does not contain information about q or p* for the α-data.

The next main part will again be dedicated to *single tubes*, and the sequence of discussion will be as before by analyzing the influences of q and p* first and then that of thermophysical properties of the fluid.

3. COMPARISON OF PREDICTION METHODS FOR NUCLEATE BOILING ON SINGLE HORIZONTAL TUBES

In this section, 8 prediction methods (listed in Table 1) from the literature for nucleate boiling heat transfer are compared with the method and the experimental data bank in the Heat Atlas. In Gorenflo et al. (2004), 5 of the 9 methods were reviewed (#1,3,4, a slightly different version of #8, and the former version of #9), and a detailed assessment of the semi-mechanistic methods of #6 & 7 has been given recently by Kenning et al. (2009). The general features of the methods are:

{Here Table 1}

Table 1. Selection of prediction methods for nucleate pool boiling heat transfer

- a power law similar to Eq(2), for the influence of the heat flux (all of the methods #1-9),
- an explicit term of p* for the influence of the pressure (#1-5 & 9) and for two of them an additional term with pressure dependent properties (#3 & 5),
- pressure dependence of α modeled only by properties of the fluid (#6-8), and
- an explicit term for the influence of surface roughness of the heater (#1, 2, 4, 9).

The discussion of the methods will be organized as in Section 2, without the part on the influence of roughness, however, because this has already been done in 2.4. Some abbreviations existing only in Table 1 have not been included in the nomenclature of the paper, but are explained within the table.

3.1 Influence of heat flux and pressure

The α(q)-dependence is shown in the n(p*)-representation at the top of Fig.11. For 6 of the methods, the exponent n of the heat flux in Eq(2) is independent of pressure, with values well below the shaded area of the main experimental scatter up to about p* = 0.1 for 5 (#1, 5-8). For # 4, n = 0.8 is crossing the shaded area from its lower limit at very small (sub-athmospheric) pressures to its upper near p* = 0.6. For two of the methods, n is decreasing with rising p*, with values near the lower limit of the experimental scatter throughout the p*-range for one (#2) and for the other (#3), n(p*) and α(p*) will be discussed separately in Fig.12.

{Here Fig.11 (width should not be reduced below about 110mm because of the many different data given)}

Fig.11: Pressure dependence of n and relative pressure dependence of α for the correlations in Table 1 and comparison with the (approximate) experimental scatter of the review in Fig.3 (shaded)

The pressure dependence of α is represented in the middle of Fig.11 for those (3) methods that contain an explicit term with p* as the Heat Atlas-method # 9. For two (#1 & 4), the pressure dependence is significantly weaker than for the experimental database, while the relative α(p*)-dependence of the third (#2) remains within the experimental scatter for p* < 0.4 and follows approximately its lower limit for higher p*. This holds for the *former* Heat Atlas correlation in a similar way, however with less pronounced deviations from the centre of experimental scatter (cf. Fig. 3, upper diagram).

In the lowest diagram of Fig.11, α/α_0 calculated for Methanol & R152a using 3 methods with pressure dependent thermophysical properties is compared with the experimental data of Fig.2 for the two fluids. The result for # 7 is similar to # 1 & 4 in the middle. For # 6, the pressure dependence is significantly too weak at very small p*, while it remains within the experimental scatter for p* > 0.2. The α(p*)-dependence of # 5 is even stronger than in the Heat Atlas method at high p* > 0.6, and for low p*, it is approximately following the upper limit of the shaded area.

For # 8, deviations from experimental values are small near atmospheric pressure, while its relative pressure dependence is too weak at higher pressures. Therefore it had been recommended in the Heat Atlas up to 2010 to calculate α-values for p* = 0.03, lying near p_{atm} for many organic fluids, and to use F(p*) of Eq.(3) to determine α_0 at $p^*_0 = 0.1$. All statements about # 8 in the next section hold for this combination with method # 9.

For method # 3, n(p*) and α(p*) are represented separately in Fig.12 (which has been extended from Kotthoff, Gorenflo, 2008). The pertaining measurements with 8 refrigerants and 4 hydrocarbons are restricted, however, to the constant temperature T_s = 7°C. Whereas the relative pressure dependence of α for the measurements agrees well with Eq(3) and the shaded area of Fig.2 in the upper diagram, the experimental or calculated n(p*)-dependence (symbols or dot-dashed line in the lower) follows the *former* n(p*)-correlation of the Heat Atlas, but only for small p* up to about 10% of p_c. For higher p*, the n-values become definitely too small. (For the method that was used to generate the relative pressure dependence of α in the upper diagram from experimental data at *a single* pressure for each fluid, see Kotthoff, Gorenflo (2008) and Kotthoff (2014).)

{Here Fig.12. (It may be reduced in size to one column = width of 84mm.)}

Fig.12: n(p*)- and relative α(p*)-dependence for the measurements of Jung et al. (2003, 2004) for 8 refrigerants and 4 hydrocarbons at constant T_s = 7°C listed in the literature review, and comparison with the results of Fig.2 (from Kotthoff, Gorenflo (2008), extended)

The experimental α_0-values of Jung's group at p* = 0.1 are systematically smaller than according to the update, see the discussion for the closed small symbols in Fig.7. The α(p*)-dependence of their method # 3 is becoming very strong for p* > 0.5, and differences in α, e.g. between Methane and Heptane rise up to 50 or 100%, see Kotthoff, Gorenflo (2008). Both aspects indicate that extrapolation to high p* would predict too high α-values and that the influence of the thermophysical properties of the fluids in this method should be revised. Therefore, it has not been considered in the next section.

3.2 Influence of thermophysical properties at p^*_0

In Tables 2 and 3, the deviations between the experimental database of the Heat Atlas and the α_0-values calculated with 7 of the methods (except # 3 & 4) are listed in the form $\Delta\alpha/\alpha_{0,exp}$. (Method # 3 has already been analyzed above, and method # 4 will be treated separately at the end of the section.) In Table 2 and Fig.13 the mean relative deviations are presented for each of the prediction methods, sub-divided into updated/non-updated/all fluids, and in Table 3 the individual deviations and $\alpha_{0,exp}$-values are given for each of the 55 fluids of the data bank. The new refrigerant R1234yf was not included because experimental data is scarce, and Helium cannot be included because q_0 = 20kW/m² is too high for nucleate boiling of this fluid.

{Here Table 2 }

Table 2. Mean relative deviations of calculated from experimental α_0-values for updated/non updated/all fluids of Table 3

{Table 3 on page following Table 2, and Fig.13 (reduced in size to one column) below Table 3 }

Table 3. Relative deviations (%) of calculated from experimental α_0-values at q_0, p^*_0, R_{a0} on copper heaters for the fluids of the Heat Atlas data bank and 7 of the 9 prediction methods in Table 1

Fig.13: Bar chart of the mean deviations for 6 of the prediction methods in Table 2

The figures for the mean deviations in terms of the absolute value for the 7 methods included in Table 2 (#1,2,5-9) reveal that the deviations are highest for # 1 or with comparatively small differences for 3 methods, either on an intermediate (#2,5,6) or low level (#7,8,9), respectively. The separation of the latter 6 in these two groups is more easily visible from the bar chart of Fig.13, with deviations around 10% for updated or all fluids, respectively, in case of the 3 methods on the right and around 20% for the other 3. It is remarkable for # 1 or 6 that almost no fluids are underpredicted or overpredicted, respectively. For engineers in practice, the latter is more desirable because it results in design "on the safe side".

In case of # 9, it is remarkable on the other hand that mean deviation of the updated fluids is very small (4.2%), while that of the non-updated is more than 3 times as high (14.9%, see also Table 3). Preferred fitting of Eq(6) to the updated could be used as an argument, but the effect will be limited, (a) because the P_f-range for the updated is much smaller than for the non-updated fluids (Fig.6) and (b) because there are only 2 fitting parameters in Eq(6) (in case of # 3, 6, 8, the situation would be different because much more fitting parameters for the thermophysical properties are involved, see Table 1). In fact, it is more likely that new

experimental results for the non-updated fluids will reduce their deviations which are mostly to the lower, see also the explanations for the lower diagram of Fig.6.

In the following, the predicted α_0-values for 7 of the methods listed in Table 1 are compared with the experimental values of the Heat Atlas data bank given in Table 3, first column on the left. Except for methods # 1 & 2 in Fig.14, that contain only the molar mass M as fluid property (besides p_c in p*), the predictions of the 5 others are also compared with the $\alpha_0(P_f)$-relationship of the Heat Atlas method, Eq(6), and plotted over the characteristic parameter P_f of the fluids according to Eq(4) in Figs.15 to 17.

Prediction methods # 1 & 2 of Cooper (1984) or Ribatski and Saiz Jabardo (2003): The comparison of these methods in Fig.14 shows (a) the identical $\alpha(M^{-0.5})$-relationship and (b) the parallel shift of both methods with # 2 being much closer to most of the experimental values, cf. calculated full straight lines or big symbols, respectively, in the lower diagram.

Besides that there appear two contrasting tendencies: On the one hand, the experimental data for the updated alcohols (A_1 – A_4) and hydrocarbons (C_1 – C_7, except for C_2) follow the $\alpha(M^{-0.5})$-relation of the two methods within narrow limits of error – with the systematic deviations in the *absolute* values, however, which have already been mentioned in (b), see the full or dashed parallel straight lines. On the other hand, there exist (c) *great differences* in experimental α_0-values *for the same molar mass* (vertical lines with tips) or (d) *very small differences* in the α-values of refrigerants *over a wide range of M*, see the halogenated C_1 – C_4 derivatives within the shaded area. This demonstrates that it is not sufficient to use only M for modeling the influence of the thermophysical properties on α at $p^*_0 = 0.1$.

{Here Fig.14 (width should not be reduced below about 120mm because of the many different data given)}

Fig.14: Comparison of experimental and calculated α_0-values for prediction methods # 1 & 2 of Cooper (1984) and Ribatski, Saiz Jabardo (2003)

Methods # 5 & 8 of Cornwell, Houston (1994) or Stephan, Preusser (1979) combined with F_{p^*} of #9: For **method # 5** which is one of those with *intermediate* mean deviations in the bar chart of Fig.13, two systematic effects appear in the upper big diagram of Fig.15: (a) Almost all heat transfer coefficients calculated for $P_f < 1.5(\mu mK)^{-1}$ fall in the same narrow range of α_0-values between about 3.2 & 4.5kW/m^{2}K. And (b) α_0-values calculated for $1 < P_f < 3.2(\mu mK)^{-1}$ are increasing systematically from about 4 to 6.5kW/m^{2}K for R152a or CH_4 at $P_f = 1.3$ or $3.15(\mu mK)^{-1}$, respectively. The cryogens with $P_f > 4(\mu mK)^{-1}$ would be underpredicted, with distances to the experimental values increasing from O_2 to H_2. These fluids are lying, however, beyond the range of validity given by Cornwell, see the dashed vertical line in the upper diagrams.

For the **combined method # 8**, the deviations in the lower two diagrams of Fig.15 are *small* throughout the (P_f)-range from 0.5 to 20 $(\mu mK)^{-1}$ without systematic effects for the different groups of fluids (except for some systematic overprediction that can be seen for small hydrocarbons).

{Here Fig.15 (width should not be reduced below about 130mm because of the many different data given)}

Fig.15: Deviations between experimental and calculated α_0-values for Cornwell/Houston prediction method (upper two diagrams) and Stephan/Preusser prediction method combined with F(p*) of method #9 (lower two diagrams), and comparison of both with $\alpha_0(P_f)$-relationship of VDI Heat Atlas

Methods # 6 & 7 of Yagov (2009) and Shekriladze (2008): In the development of both of these methods, Eq(5) is included. Therefore, a systematic influence of P_f should appear in the calculated α_0-values. And in fact, this is clearly evident from all the $\alpha_0(P_f)$-diagrams of Fig.16. In addition, almost all values calculated from **method # 6** are lying in very narrow α-ranges around the boldly dashed straight lines which are shifted downwards *for -20%* from Eq(6) in the upper diagrams. Two consequences are following for this method: (a) Overprediction occurs only for 5 fluids, see the 5 coloured vertical arrows. (b) For some of the non-updated refrigerants with approximately the same *experimental* deviations of -20% from Eq(6) (big open squares), the deviations of the calculated values (small open squares) are somewhat smaller than for the other fluids.

For **method # 7** with *small* mean deviations in the bar chart, the differences between predicted and experimental α_0-values in the lower diagrams of Fig.16 are *particularly small* for almost all hydrocarbons (small diamonds with or without dashes) and most of the non-updated refrigerants (small open squares). On the other hand, systematic deviations *downwards* exist for the calculated values of many *updated* refrigerants (small squares with dashes).

{Here Fig.16 (width should not be reduced below about 130mm because of the many different data given)}

Fig.16: Deviations between experimental and calculated α_0-values for Yagov prediction method (upper three diagrams) and Shekriladze prediction method (lower three diagrams), and comparison of both with $\alpha_0(P_f)$-relationship of VDI Heat Atlas

Method # 4 of Nishikawa, Fujita, Ohta, Hidaka (1982): The only properties of the fluid included in this method are M, p_c, and T_c. Therefore, the result of Fig.17 had not been expected that ***the data calculated by method #4*** (small symbols in both diagrams) can also be interpolated ***by a uniform power law of α_0 with P_f*** corresponding to Eq(6), see the *bold* straight interpolation lines in both diagrams. Any deviations beyond the narrow limits of scatter given in the diagrams (dashed lines for ±10% running parallel to the bold full lines) exist merely for Neon, Methanol and Ethanol. The only differences of the modified $\alpha_0(P_f)$-power law to Eq(6) are the new fitting parameters of factor $A = \alpha_{ref} = 4.4 kW/m^2K$ and exponent m = 0.815. As can be seen from the lower diagram, the modified correlation and Eq(6) are coinciding near $\alpha_0 = 2 kW/m^2K$.

{Here Fig.17 (width should not be reduced below about 130mm because of the many different data given)}

Fig.17: Deviations between experimental and calculated α_0-values for Nishikawa, Fujita prediction method and comparison with $\alpha_0(P_f)$-relationship of VDI Heat Atlas

The **differences between measured and calculated α_0-values** (big or small symbols) are increasing for rising P_f, with only a few exceptions: the updated alcohols in the upper, and water, ammonia and some of the non-updated refrigerants in the lower diagram of Fig.17. It seems that the deviations may result from fitting the correlation of method #4 particularly to water and ammonia as follows from the vanishing deviations between measurement and calculation for these fluids (big and small circles in the lower diagram).

On the other hand, a closer look at the updated hydrocarbons, HFC-refrigerants and alcohols in the upper diagram of Fig.17 reveals that deviations between α_0-values *calculated by method #4 or a modified $\alpha_0(P_f)$-power law, respectively,* will become extremely smaller than the overall scatter of ±10% given for the two prediction methods, if the power law will be fitted *individually* to each of the 3 groups of fluids: Modifying the (overall) factor of 4.4 to 4.63 or 4.23 for hydrocarbons or refrigerants, respectively, results in the two dotted straight lines running parallel to the bold full line. The individual fits have reduced the maximum scatter to ±3% for hydrocarbons (+3.2% for Propane or -2.9% for Cyclohexane) and ±3.5% for HFC-refrigerants (+3.5% for R32 or -3.5% for R227). For the other halocarbon refrigerants in Table 2, deviations are only slightly higher, if the former mixture R502 is not taken into account, with maxima of +4.3% for R13B1 or -4.0% for R14. For CO_2, deviations do not exceed 5%, if any of the three factors is used.

In case of the alcohols, the slope of the dotted straight line is significantly less pronounced than for the two other families of fluids, so *both* fitting parameters have to be modified to $\alpha_{ref} = 4.08 kW/m^2K$ and m = 0.388. As a result, deviations between the two calculation methods are least, with maxima of +1.4% for 2-Propanol or -1.3% for Ethanol. And for the two non-updated alcohols of Table 2, only one of the deviations is slightly higher (+1.3% for n-Butanol and -1.7% for i-Butanol).

Above all, the very small scatter between the small symbols calculated by method #4 and each of the 3 pertaining dotted lines calculated by $\alpha_0(P_f)$-relationships reveals that a close relation seems to exist between the excess pressure within a bubble at vapour/liquid equilibrium and thermodynamic properties at the Critical State, at least for substances within the same family of fluids. Therefore, it should be worthwhile to investigate further in the relation between the definition of P_f in Eq(4) and the combination of M, p_c, and T_c, in this prediction method. Similar combinations of M, R, p_c, and T_c had often been used by Soviet researchers more than 50 years ago to model the absolute values of α in pool boiling heat transfer.

Finally, the other part of the influence of thermophysical properties will be discussed again that is represented by the factor F_{p^*} in Eq(1) or the empirical function of the reduced pressure in Eq(3), respectively, and it is tried to model also this part by means of the fluid parameter P_f . In a first attempt, P_f is applied to the data set in Fig.2 for the fluids of the own measurements. The mixture R507 has been excluded from the 23 fluids investigated because the standardized composition of this mixture (50/50 mass-% of R125/R143a) forms an azeotrope at *low* saturation temperature so data at *high* reduced pressures might be influenced by slightly *zeotropic* behavior.

{Here Fig.18 (width should not be reduced below about 150mm because of the many different data given)}

Fig.18: Representation of the relative pressure dependence of α in terms of the fluid parameter P_f for the fluids of Fig.2 (without the mixture R507)

In Fig.18, the heat transfer coefficients α for the entire experimental pressure range – indicated by the inserted p*-scale – have been reduced by their values at $p^*_0 = 0.1$ as in the lower diagram of Fig.2. The fluid parameter P_f has also been reduced by its value at p^*_0 to form $P_f^* = P_f/P_{f,0}$, with $P_f = [(dp/dT)_{VPC} /\sigma]$ at variable reduced pressure p* and $P_{f,0}$ at $p^*_0 = 0.1$. The bold straight line for

$$\alpha^* = P_f^{*0.6} \qquad (9)$$

corresponds to Eq(6), and the experimental data from about atmospheric pressure up to p* = 0.8 are represented fairly well by the power law of Eq(9), with deviations exceeding the limits of ±10% only in a few cases.

Thus, the influence of thermophysical properties on α, which above was separated more or less arbitrarily in two parts, is combined again, and the two functions F_{p^*} and F_f in Eq(1) may be replaced by Eq(9). This is plausible for the pressure range near p^*_0 because the same (kind of) cavities within the roughness structure of the heated surface will be activated as nucleation sites, either at p^*_0 = const or at somewhat higher or lower p*, respectively. Having in mind that the size of potential nucleation sites is getting smaller and smaller with increasing reduced pressure, it is by no means a matter of course, however, that the power law found for p^*_0 = 0.1 will hold up to the highest pressures investigated.

Instead, an additional influence of the size distribution of the cavities on the heated surface should appear. Maybe, the special treatment of the tubes used for the experiments of Fig.2 or 18, respectively, by sandblasting twice and with different blasting pressures and grain sizes has produced plenty of potential nucleation sites of *all sizes needed* up to p* = 0.8 (and higher, see Gorenflo et al., 2010).

For *very low reduced* pressures, however, effects connected with the *vigorous convection* induced by the (few) big fast-growing and fast-moving bubbles that can be seen on videos from this pressure range will become dominating and nucleation-controlled heat transfer which is governed by Eq(5) will lose importance. And indeed, the relative increase of α with P_f is *significantly different* and less pronounced in this pressure range for the measurements of methanol at the lowest two pressures which are sub-atmospheric (see the left vertical arrow for p_{atm}) – and also for those at the two higher pressures which, however, can also be interpolated (almost equally well) by the stronger relative increase of α with P_f in Eq(9).

Nevertheless, the remaining relative pressure dependence at low p* is significantly more pronounced than the very weak increase of α with p* for single-phase free convection which is governed by the density difference of the liquid between the heated boundary layer and the pool. And the more pronounced α(p*)-dependence of this kind of convection is consistent with the fact that it is induced by the big bubbles at low p* because both, size of the bubbles and their local density on the heated wall depend on p*.

The very first interpretation given above for the entire $\alpha^*(P_f^*)$-relation shown in Fig.18, which results merely from the own measurements with two tubes of similar surface treatment, should be checked carefully by further detailed comparisons with the relative increase of α with P_f following from other coherent experimental data sets.

4. CONCLUSIONS

The comparison of various prediction methods for nucleate boiling heat transfer has shown that prediction of the influences of heat flux q, reduced pressure p*, and properties of the fluid on α is already comparatively safe. Knowledge of the influence of the heater, however, should be improved with very first priority, also because it is connected with the influences of p* and particularly of q, because the strict separation of the various influences as has been done in Eq(1) – except for the p*-dependence of n – is only a first approach. And for better interpretation of the influence of thermophysical properties of the fluid, more accurate experimental data on surface tension are needed for most of the fluids important in industrial applications of pool boiling.

REFERENCES

Bier, K., Gorenflo, D., Wickenhäuser, G., 1973. Zum Wärmeübergang beim Blasensieden in einem weiten Druckbereich. Chem.Ing.Techn. 14, 935-942.

Bier, K., Gorenflo, D., Wickenhäuser, G., 1977. Pool boiling heat transfer at saturation pressures up to critical. In: Heat Transfer in Boiling, Hem.Publ.Corp.,Washington, London, 137-158.

Bier, K., Lambert, M., 1990. Heat transfer in nucleate boiling of different low boiling substances. Int. J. Refrigeration 13, 293-300; cf. also: Lambert, M., Wärmeübergang beim Blasensieden im Bereich tiefer Siedetemperaturen. PhD thesis, Univ. Karlsruhe (TH).

Buljina, I., 2010. Entwicklung und Aufbau zweier Siedeapparaturen zur Untersuchung des Wärmeübergangs weitsiedender binärer niedrig- und hochviskoser Gemische. PhD thesis, Ruhr-Univ. Bochum.

Cooper, M.G., 1984. Heat flow rates in saturated nucleate pool boiling – a wide ranging examination using reduced properties. Adv. in Heat Transfer, Vol.16.

Cornwell, K., Houston, S.D., 1994. Nucleate pool boiling on horizontal tubes: a convection-based correlation. Int. J. Heat Mass Transfer 37, 303-309.

Danger, E., 2004. Wärmeübergang und Blasenbildung beim Sieden. PhD thesis, Univ. Paderborn, DKV-Forschungsbericht Nr.70.

Dhir, V.K., 2006. Mechanistic prediction of nucleate boiling heat transfer – achievable or a hopeless task? J. Heat Transfer 128, 1-12.

Gorenflo, D., 1977. Wärmeübergang bei Blasensieden, Filmsieden und einphasiger freier Konvektion in einem grossen Druckbereich. Abh. Deutscher Kälte- und Klimatechn. Verein Nr.22, C.F.Müller, Karlsruhe.

Gorenflo, D., 1984. Behältersieden. Kap. Ha, 4th – 6th ed & Hab, 7th - 10th ed, Springer, Berlin, Heidelberg.

Gorenflo, D., Sokol, P., Caplanis, S., 1990. Pool boiling heat transfer from single plain tubes to various hydrocarbons. Int. J. Refrigeration 13, 286-292.

Gorenflo, D., Sokol, P., Caplanis, S., 1991. Zum Wärmeübergang beim Blasensieden von Kohlenwasser-stoffen und Halogen-Kältemitteln an einem Glattrohr und einem Hochleistungs-Rippenrohr. Wärme- und Stoffübertragung 26, 273-281.

Gorenflo, D., Luke, A., Danger, E., 1998. Interactions between heat transfer and bubble formation in nucleate boiling. Proc. 11th Int. Heat Transfer Conf., Kyongju, Vol.1, 149-174.

Gorenflo, D., Chandra, U., Kotthoff, S., Luke, A., 2004. Influence of thermophysical properties on pool boiling heat transfer of refrigerants. Int. J. Refrigeration 27, 492-502.

Gorenflo, D., Baumhögger, E., Windmann, T., Herres, G., 2010. Nucleate pool boiling, film boiling and single-phase free convection at pressures up to the critical state, Part I & II. Int. J. Refrigeration 33, 1229-1263.

Gorenflo, D., Kenning, D.B.R., 2010. Pool Boiling. Chapter H2, VDI-Heat Atlas, 2nd ed. Springer, Berlin.

Gorenflo, D., Kotthoff, S., Baumhögger, E., Herres, G., 2012. Aktualisierte Wärmeatlas-Rechenmethode – Auslegung überfluteter Verdampfer – DKV-Tagungsbericht 38, Bd.II.1.

Gorenflo, D., 2013. Behältersieden. Kapitel H2, 11th ed, Springer, Berlin, Heidelberg.

Gremer, F., 2001. Phasengleichgewicht & Wärmeübergang beim Sieden von Mehrstoffsystemen aus Wasser und Alkoholen. PhD thesis, Univ. Paderborn.

Jung, D., Kim, Y., Ko, Y., Song, K.H., 2003. Nucleate boiling heat transfer coefficients of pure halogenated refrigerants. Int. J. Refrigeration 26, 240-248.

Jung, D., Lee, H., Bae, D., Oho, S., 2004. Nucleate boiling heat transfer coefficients of flammable refrigerants. Int. J. Refrigeration 27, 409-414.

Kang, D.G., Park, K.J., Jung, D., 2009. Nucleate boiling heat transfer coefficients of halogenated refrigerants. Proc. 3rd IIR Conf. on Thermophysical Properties and Transfer Processes of Refrigerants, Boulder (CO), USA, paper # 195.

Kenning, D.B.R., 1999. What do we really know about nucleate boiling? I Mech E Conf. Transactions, 6th UK Nat. Heat Transfer Conf., Edinburgh, 143-167.

Kenning, D.B.R., Golobìc, I., Petkovsèc, J., 2009. Pool boiling: Global correlations and mechanistic studies. Keynote, Proc. 11th UK Nat. Heat Transfer Conf., London.

Kotthoff, S., Gorenflo, D., 2005. Influence of the fluid on pool boiling heat transfer of refrigerants and other organic substances. Proc. 2nd IIR Conf. on Thermophysical Properties and Transfer Processes of Refrigerants, Vicenza, Italy, paper TP47.

Kotthoff, S., Gorenflo, D., 2008. Pool boiling heat transfer to hydrocarbons and ammonia: A state-of-the-art review. Int. J. Refrigeration 31, 573-602.

Kotthoff, S., Gorenflo, D., 2012. Messungen zum Einfluss von Fluid- und Heizflächeneigenschaften auf Wärmeübergang und Blasenbildung beim Sieden. DKV-Tagungsbericht 38, Bd.II.1.

Kotthoff, S., 2014. Zum Einfluss von Fluid- und Heizflächeneigenschaften auf Wärmeübergang und Blasenbildung beim Sieden. PhD thesis, Univ. Paderborn.

Lemmon,E.W., Mc Linden, M.O., Huber, M.L., 2010. Refprop, Reference Fluid Thermodynamic and Transport Properties, NIST Standard Reference Database 23, Version 9.0.

Luke, A., 1996. Beitrag zum Einfluss der Mikrostruktur von Heizflächen auf den Wärmeübergang beim Blasensieden. PhD thesis, Univ. Paderborn; cf. also: 1997, Pool boiling heat transfer from horizontal tubes with different roughness. Int. J. Refrigeration 20, 561-574.

Nishikawa, K., Fujita, Y., Ohta, H., Hidaka, S., 1982. Effect of the roughness on the nucleate boiling heat transfer over wide range of pressure. Proc. 7th Int. Heat Transfer Conf., München, Vol.4, 61-66.

Park, K.J., Jung, D., 2007. Boiling heat transfer enhancement with carbon nanotubes for refrigerants used in building air-conditioning. J. Energy and Buildings 39, 1061-1064.

Park, K.J., Jung, D., 2010. Nucleate boiling heat transfer coefficients of R1234yf on plain and low fin surfaces. Int. J. Refrigeration 33, 553-557.

Ribatski, G., Saiz Jabardo, J.M., 2003. Experimental study of nucleate boiling of halocarbon refrigerants on cylindrical surfaces.Int. J. Heat Mass Transfer 46, 4439-4451.

Salem, M.I., 1979. Wärmeübergang beim Blasensieden und Grössenverteilungen von stabilen Blasenkeimen sowie von Rauhigkeitsvertiefungen der Heizfläche. PhD thesis, Univ. Karlsruhe (TH).

Schömann, H., 1994. Beitrag zum Einfluss der Heizflächenrauhigkeit auf den Wärmeübergang beim Blasensieden. PhD thesis, Univ. Paderborn.

Shekriladze, I.G., 2008. Boiling heat transfer: mechanisms, models, correlations and the lines of further research. The Open Mech. Eng. J. 2, 104-127. Update of former versions from 1981 and 1966.

Span, R., 2010. Properties at Saturation. Chapter D3.2, VDI-Heat Atlas, 2nd ed., Springer, Berlin.

Stephan, K., 1963. Mechanismus und Modellgesetz des Wärmeübergangs bei der Blasenverdampfung. Chem. Ing. Techn., 775-784; cf. also: 1964, Beitrag zur Thermodynamik des Wärmeübergangs beim Sieden. Abh. Deutscher Kälte- und Klimatechn. Verein, Nr.18, C.F.Müller, Karlsruhe.

Stephan, K., Preusser, P., 1979. Wärmeübergang und maximale Wärmestromdichte beim Behältersieden binärer und ternärer Flüssigkeitsgemische. Chem. Ing. Techn., MS, 649-679.

Stephan, P., Fuchs, T., 2009. Local heat flow and temperature fluctuations in wall and fluid in nucleate boiling systems. Heat Mass Transfer 45, 919-928.

van Royen, E., Agostini, F., Borhani, N., Thome, J.R., 2012. Boiling on a tube bundle: Part II – heat transfer and pressure drop. Heat Transfer Engineering 33, 930-946.

Yagov, V.V., 2009. Nucleate boiling heat transfer: possibilities and limitations of theoretical analysis. Heat Mass Transfer 45, 881-892. Update of a former version from 1988.

Figure captions and table headings:

Fig. 1: Concept of the calculation method shown for i-Butane boiling on a copper tube

Fig. 2: Pressure dependence of n and relative pressure dependence of α for the own new experiments with 23 fluids and comparison with the correlations of the Heat Atlas

Fig. 3: Pressure dependence of n and α for the new experiments of the literature review and comparison with the Heat Atlas calculation method. Top: Hydrocarbons (together with the overall scatter of the former experimental Heat Atlas database for organic fluids). Bottom: Refrigerants, alcohols and 3 fluids from other groups

Fig. 4: $\alpha_{0.1}(P_f)$-representation for the own new experiments with 23 fluids boiling on the two copper tubes # 1 & 2. Top: Separate diagrams for tube # 1 or # 2. Bottom: Data for both tubes compared with Eq(6) adapted to $R_{a,\,exp}$ (dashed lines) and with earlier data for 3 of the fluids boiling on a fine sandblasted 25mm-tube (#3, small symbols; from Danger, 2004)

Fig. 5: Update of the former experimental database for α_0 (big open symbols) in the Heat Atlas by new experiments (small symbols) and comparison with the updated database (shaded big symbols) and the $\alpha_0(P_f)$-correlation

Fig. 6: Comparison of the $\alpha_0(P_f)$-correlation with the new experimental database of the Heat Atlas

Upper two diagrams: updated fluids; lower two diagrams: non-updated fluids and H_2O, NH_3

Fig.7: $\alpha_0(P_f)$-dependence for discussion of new measurements with n-Butanol and the new refrigerant R1234yf

Fig.8: Relative differences $\Delta\alpha$ for copper tubes with different surface roughness:
Comparison of measurements (partly closed symbols and full lines) with calculated data for 4 of the prediction methods in Table 1 of Section 3 (open symbols and dot-dashed lines)

Fig.9: $\alpha(q)$-dependency for R134a and the new refrigerant R1234yf boiling on flat plain or finned copper plates (from Park, Jung, 2010, extended)

Fig.10: $\alpha(q)$-dependency for R134a (upper diagram) and the new refrigerant R236fa (lower diagram) boiling on a bundle of horizontal copper tubes at 4 saturation temperatures between 5 and 20°C.

Big symbols and dashed straight interpolation lines: experimental data from (van Royen et al., 2012).

Small symbols and full curves or straight lines: calculated data for a bundle or single tubes, respectively, from Heat Atlas prediction method.

Fig.11: Pressure dependence of n and relative pressure dependence of α for the correlations in Table 1 and comparison with the (approximate) experimental scatter of the review in Fig.3 (shaded)

Fig.12: n(p*)- and relative α(p*)-dependence for the measurements of Jung et al. (2003, 2004) for 8 refrigerants and 4 hydrocarbons at constant $T_s = 7^oC$ listed in the literature review, and comparison with the results of Fig.2 (from Kotthoff, Gorenflo (2008), extended)

Fig.13: Bar chart of the mean deviations for 6 of the prediction methods in Table 2

Fig.14: Comparison of experimental and calculated α_0-values for prediction methods # 1 & 2 of Cooper (1984) and Ribatski, Saiz Jabardo (2003)

Fig.15: Deviations between experimental and calculated α_0-values for Cornwell/Houston prediction method (upper two diagrams) and Stephan/Preusser prediction method combined with F(p*) of method #9 (lower two diagrams), and comparison of both with $\alpha_0(P_f)$-relationship of VDI Heat Atlas

Fig.16: Deviations between experimental and calculated α_0-values for Yagov prediction method (upper three diagrams) and Shekriladze prediction method (lower three diagrams), and comparison of both with $\alpha_0(P_f)$-relationship of VDI Heat Atlas

Fig.17: Deviations between experimental and calculated α_0-values for Nishikawa, Fujita prediction method and comparison with $\alpha_0(P_f)$-relationship of VDI Heat Atlas

Fig.18: Representation of the relative pressure dependence of α in terms of the fluid parameter P_f for the fluids of Fig.2 (without the mixture R507)

Table 1. Selection of prediction methods for nucleate pool boiling heat transfer

Table 2. Mean relative deviations of calculated from experimental α_0-values for updated/non updated/all fluids of Table 3

Table 3. Relative deviations (%) of calculated from experimental α_0-values at q_0, p_0^*, R_{a0} on copper heaters for the fluids of the Heat Atlas data bank and 7 of the 9 prediction methods in Table 1

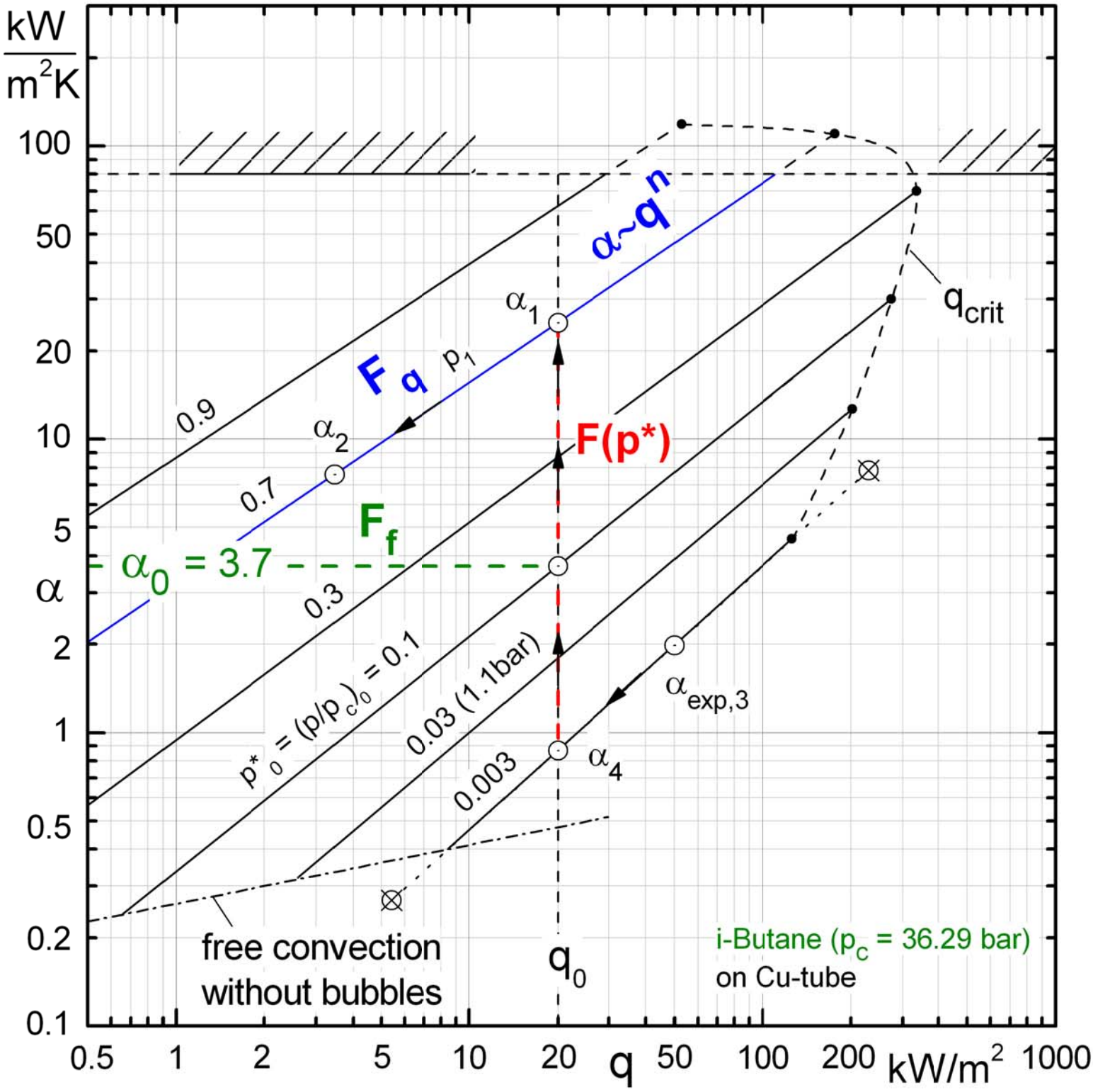
kW
m²K
100
50
20
10
5
α
2
1
0.5
0.2
0.1
0.5
1
2
5
10
20
q
50
100
200
kW/m²
1000
α~q^n
α1
α2
F q p1
F(p*)
Ff
α0 = 3.7
0.9
0.7
0.3
p*0 = (p/pc)0 = 0.1
0.03 (1.1bar)
0.003
α4
αexp,3
qcrit
q0
free convection
without bubbles
i-Butane (pc = 36.29 bar)
on Cu-tube

Figure 1

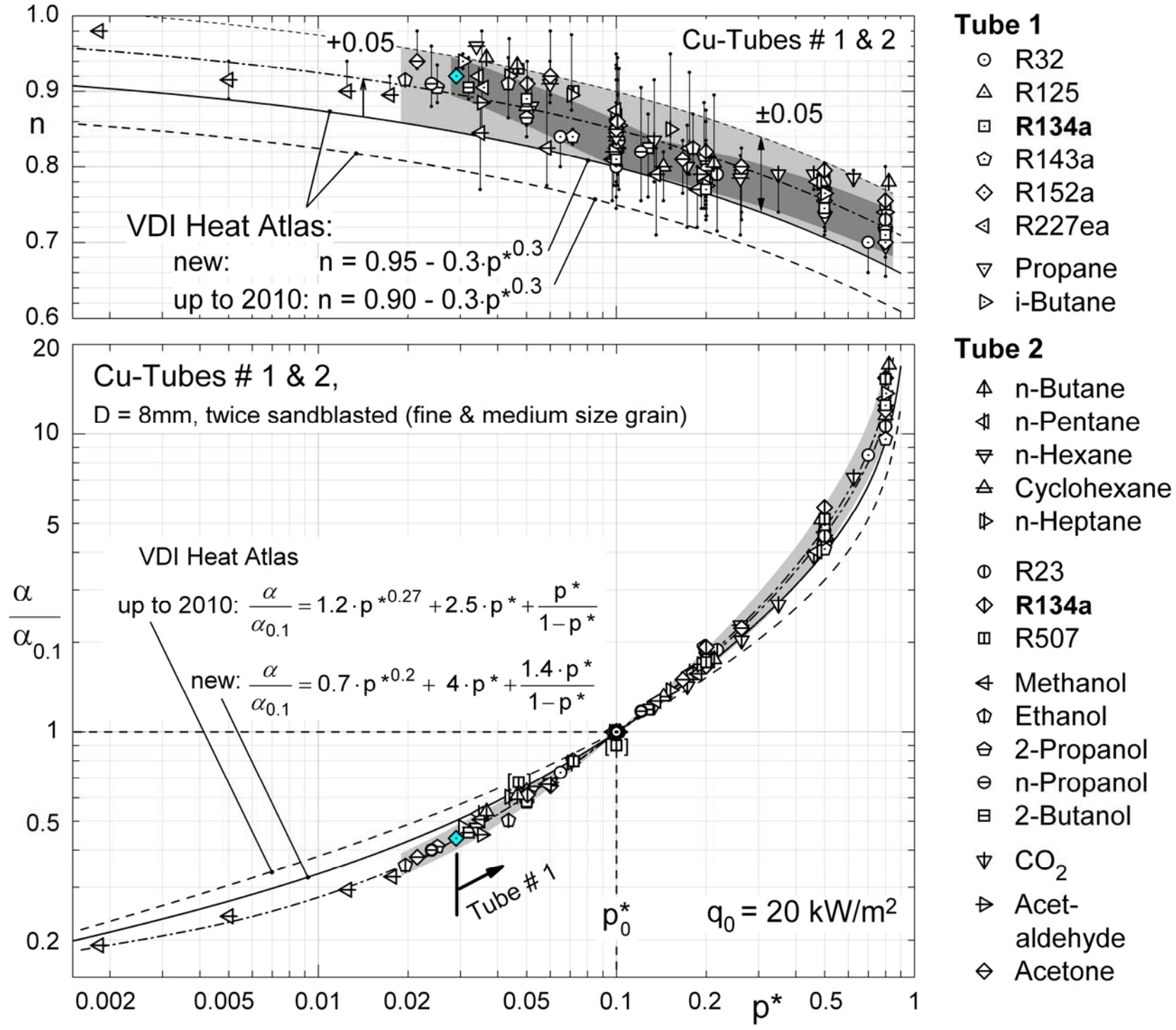
Cu-Tubes # 1 & 2
+0.05
±0.05
n
VDI Heat Atlas:
new: n = 0.95 - 0.3·p*^0.3
up to 2010: n = 0.90 - 0.3·p*^0.3
Cu-Tubes # 1 & 2,
D = 8mm, twice sandblasted (fine & medium size grain)
VDI Heat Atlas
up to 2010: α/α0.1 = 1.2·p*^0.27 + 2.5·p* + p*/(1−p*)
new: α/α0.1 = 0.7·p*^0.2 + 4·p* + 1.4·p*/(1−p*)
Tube # 1
p*0
q0 = 20 kW/m²
α/α0.1
p*
Tube 1
R32
R125
R134a
R143a
R152a
R227ea
Propane
i-Butane
Tube 2
n-Butane
n-Pentane
n-Hexane
Cyclohexane
n-Heptane
R23
R134a
R507
Methanol
Ethanol
2-Propanol
n-Propanol
2-Butanol
CO2
Acet-aldehyde
Acetone

Figure 2

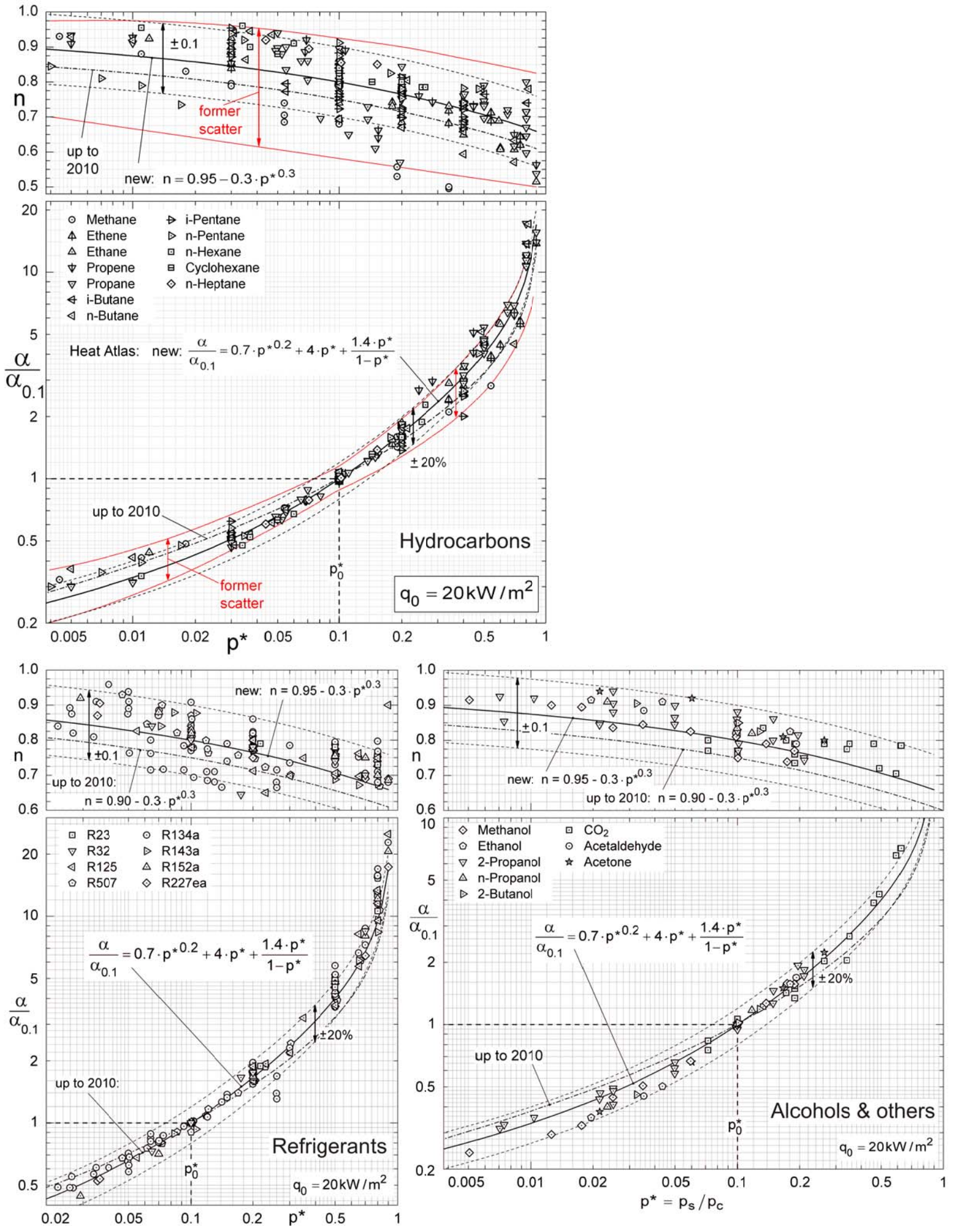
n
±0.1
former scatter
up to 2010
new: n = 0.95 − 0.3 · p*^0.3
Methane
Ethene
Ethane
Propene
Propane
i-Butane
n-Butane
i-Pentane
n-Pentane
n-Hexane
Cyclohexane
n-Heptane
Heat Atlas: new: α/α0.1 = 0.7 · p*^0.2 + 4 · p* + 1.4 · p* / (1 − p*)
± 20%
up to 2010
former scatter
p*0
Hydrocarbons
q0 = 20 kW/m²
p*
new: n = 0.95 - 0.3 · p*^0.3
up to 2010: n = 0.90 - 0.3 · p*^0.3
R23
R32
R125
R507
R134a
R143a
R152a
R227ea
α/α0.1 = 0.7 · p*^0.2 + 4 · p* + 1.4 · p* / (1 − p*)
±20%
up to 2010:
Refrigerants
Methanol
Ethanol
2-Propanol
n-Propanol
2-Butanol
CO2
Acetaldehyde
Acetone
Alcohols & others
p* = ps / pc

Figure 3

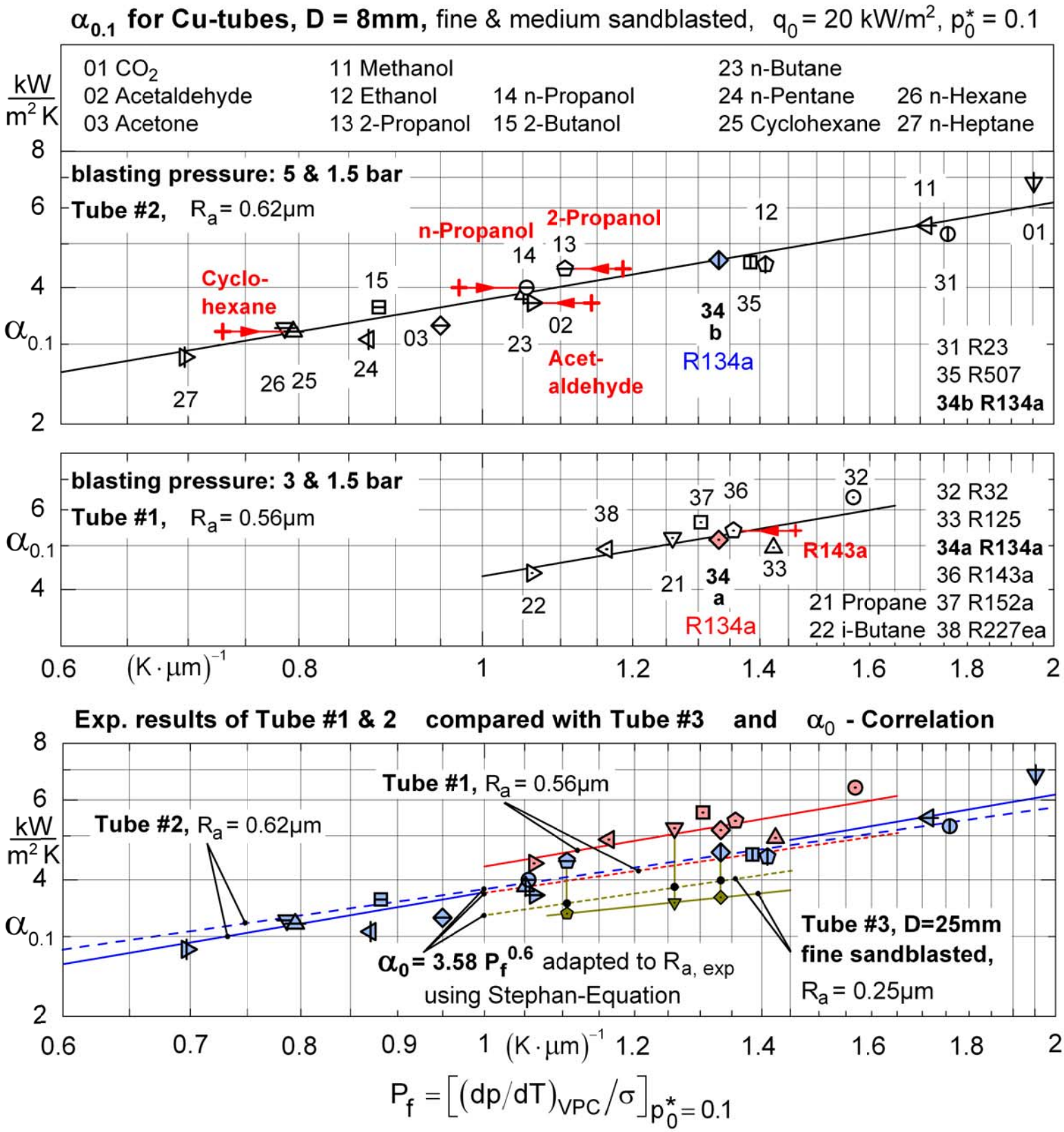
$\alpha_{0.1}$ for Cu-tubes, D = 8mm, fine & medium sandblasted, q_0 = 20 kW/m², p_0^* = 0.1
01 CO_2
02 Acetaldehyde
03 Acetone
11 Methanol
12 Ethanol
13 2-Propanol
14 n-Propanol
15 2-Butanol
23 n-Butane
24 n-Pentane
25 Cyclohexane
26 n-Hexane
27 n-Heptane
kW / m² K
blasting pressure: 5 & 1.5 bar
Tube #2, R_a = 0.62µm
Cyclo-hexane
n-Propanol
2-Propanol
Acet-aldehyde
34 b R134a
31 R23
35 R507
34b R134a
blasting pressure: 3 & 1.5 bar
Tube #1, R_a = 0.56µm
R143a
34 a R134a
32 R32
33 R125
34a R134a
36 R143a
37 R152a
38 R227ea
21 Propane
22 i-Butane
$\alpha_{0.1}$
$(K \cdot \mu m)^{-1}$

Exp. results of Tube #1 & 2 compared with Tube #3 and α_0 - Correlation
Tube #1, R_a = 0.56µm
Tube #2, R_a = 0.62µm
$\alpha_0 = 3.58\ P_f^{0.6}$ adapted to $R_{a,\,exp}$ using Stephan-Equation
Tube #3, D=25mm fine sandblasted, R_a = 0.25µm
kW / m² K
$\alpha_{0.1}$
$(K \cdot \mu m)^{-1}$
$P_f = \left[(dp/dT)_{VPC} / \sigma \right]_{p_0^* = 0.1}$

Figure 4

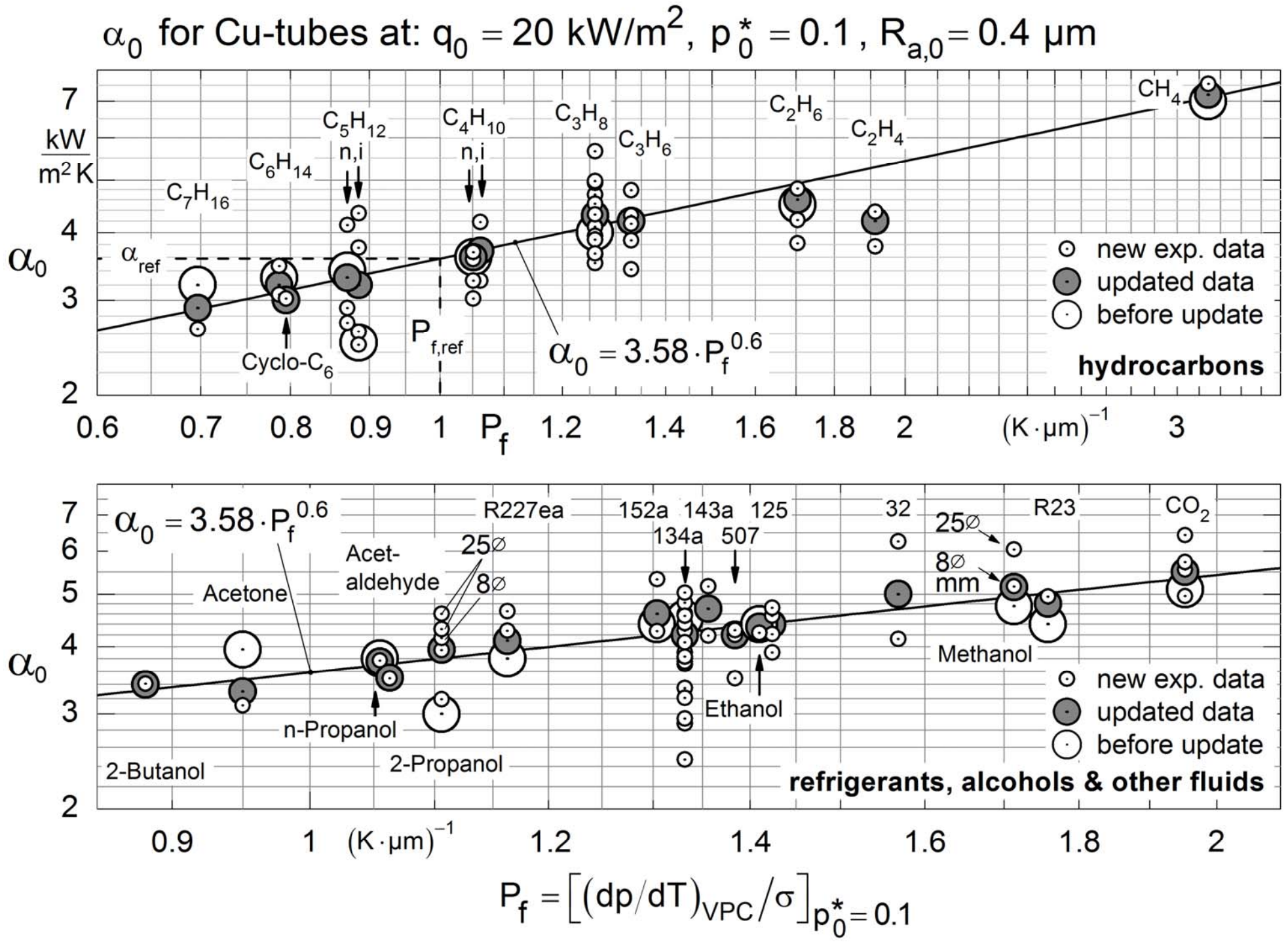
α_0 for Cu-tubes at: $q_0 = 20$ kW/m^2, $p_0^* = 0.1$, $R_{a,0} = 0.4$ µm
α_0
kW / m^2 K
C_7H_{16}
C_6H_{14}
C_5H_{12} n,i
C_4H_{10} n,i
C_3H_8
C_3H_6
C_2H_6
C_2H_4
CH_4
α_{ref}
Cyclo-C_6
$P_{f,ref}$
$\alpha_0 = 3.58 \cdot P_f^{0.6}$
new exp. data
updated data
before update
hydrocarbons
P_f
$(K \cdot \mu m)^{-1}$
$\alpha_0 = 3.58 \cdot P_f^{0.6}$
Acetone
Acet-aldehyde
25∅
8∅
R227ea
152a 143a 125
134a 507
32
25∅
8∅ mm
R23
CO_2
Methanol
Ethanol
n-Propanol
2-Propanol
2-Butanol
new exp. data
updated data
before update
refrigerants, alcohols & other fluids
$P_f = \left[(dp/dT)_{VPC} / \sigma \right]_{p_0^* = 0.1}$

Figure 5

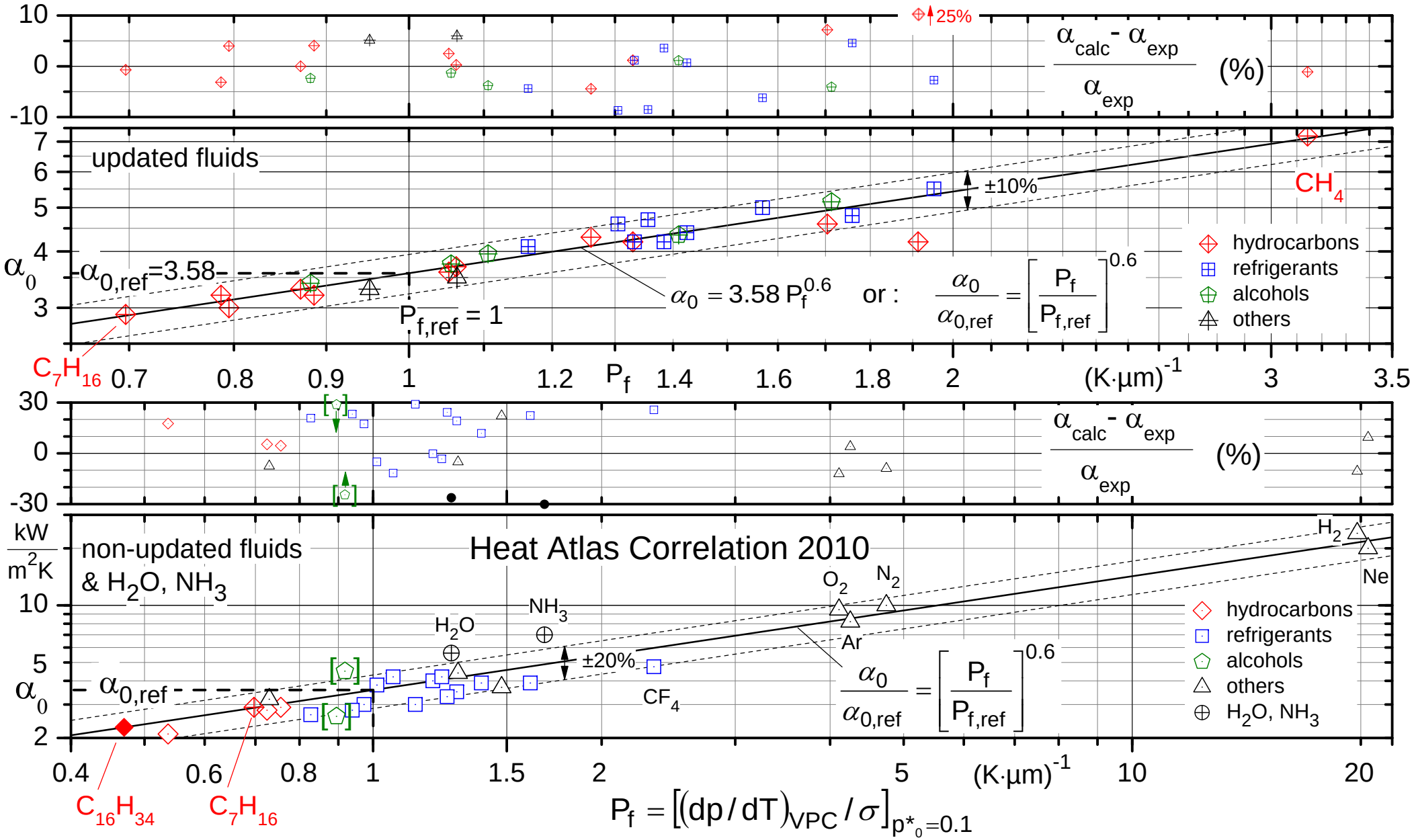
25%
(%)
updated fluids
±10%
CH4
α0,ref=3.58
α0 = 3.58 Pf^0.6
or :
Pf,ref = 1
C7H16
Pf
(K·µm)-1
hydrocarbons
refrigerants
alcohols
others
non-updated fluids
& H2O, NH3
Heat Atlas Correlation 2010
±20%
H2
Ne
O2
N2
Ar
NH3
H2O
CF4
C16H34
C7H16
Pf = [(dp/dT)VPC/σ]p*0=0.1

Figure 6

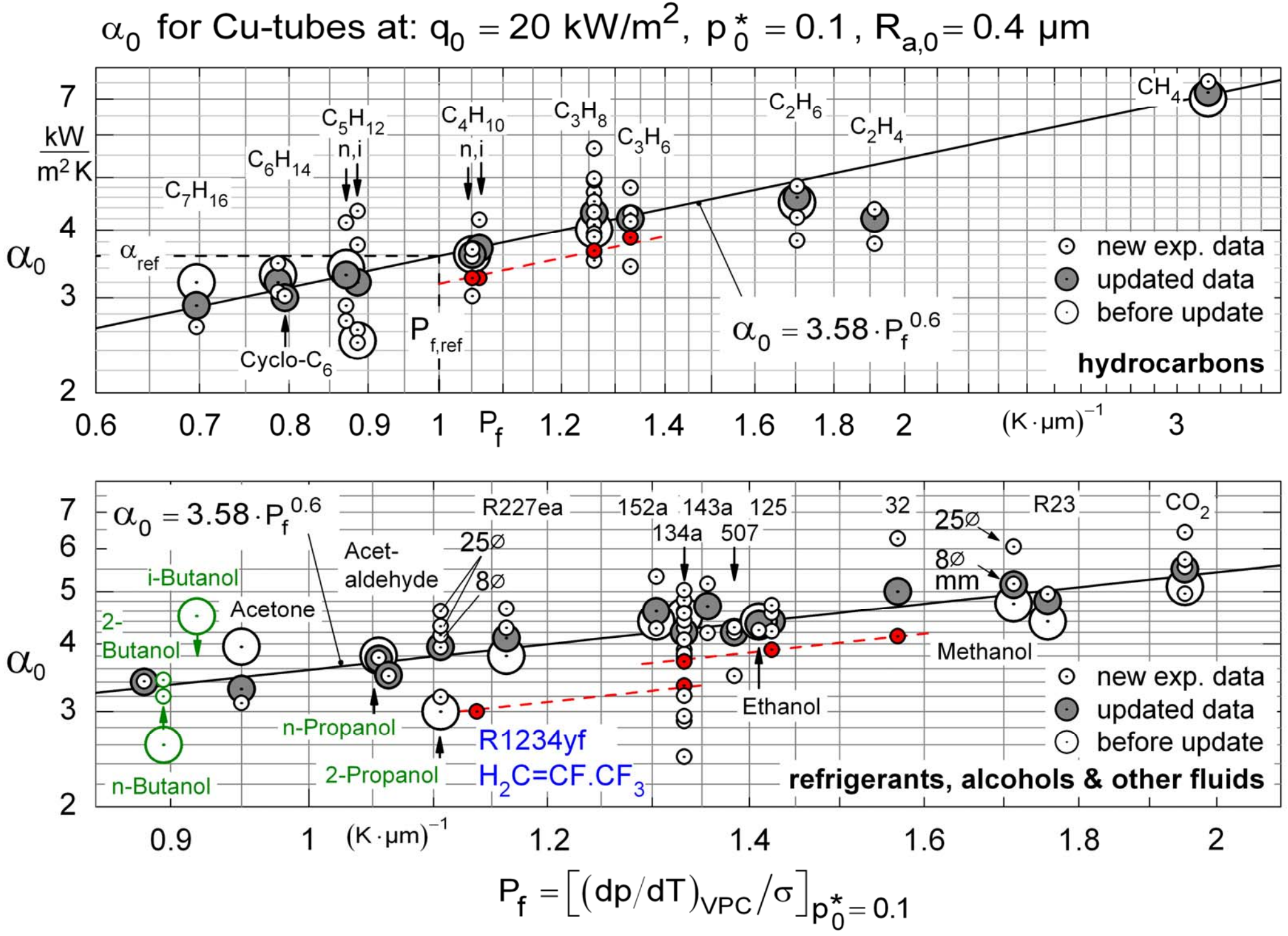
α_0 for Cu-tubes at: $q_0 = 20$ kW/m^2, $p_0^* = 0.1$, $R_{a,0} = 0.4$ µm
α_0
kW / m^2 K
C_7H_{16}
C_6H_{14}
C_5H_{12} n,i
C_4H_{10} n,i
C_3H_8
C_3H_6
C_2H_6
C_2H_4
CH_4
α_{ref}
Cyclo-C_6
$P_{f,ref}$
$\alpha_0 = 3.58 \cdot P_f^{0.6}$
new exp. data
updated data
before update
hydrocarbons
P_f
$(K \cdot \mu m)^{-1}$
$\alpha_0 = 3.58 \cdot P_f^{0.6}$
R227ea
152a
143a
125
134a
507
32
25ø
8ø
mm
R23
CO_2
i-Butanol
2-Butanol
n-Butanol
Acetone
Acet-aldehyde
n-Propanol
2-Propanol
R1234yf
$H_2C=CF.CF_3$
Methanol
Ethanol
new exp. data
updated data
before update
refrigerants, alcohols & other fluids
$P_f = \left[(dp/dT)_{VPC} / \sigma \right]_{p_0^* = 0.1}$

Figure 7

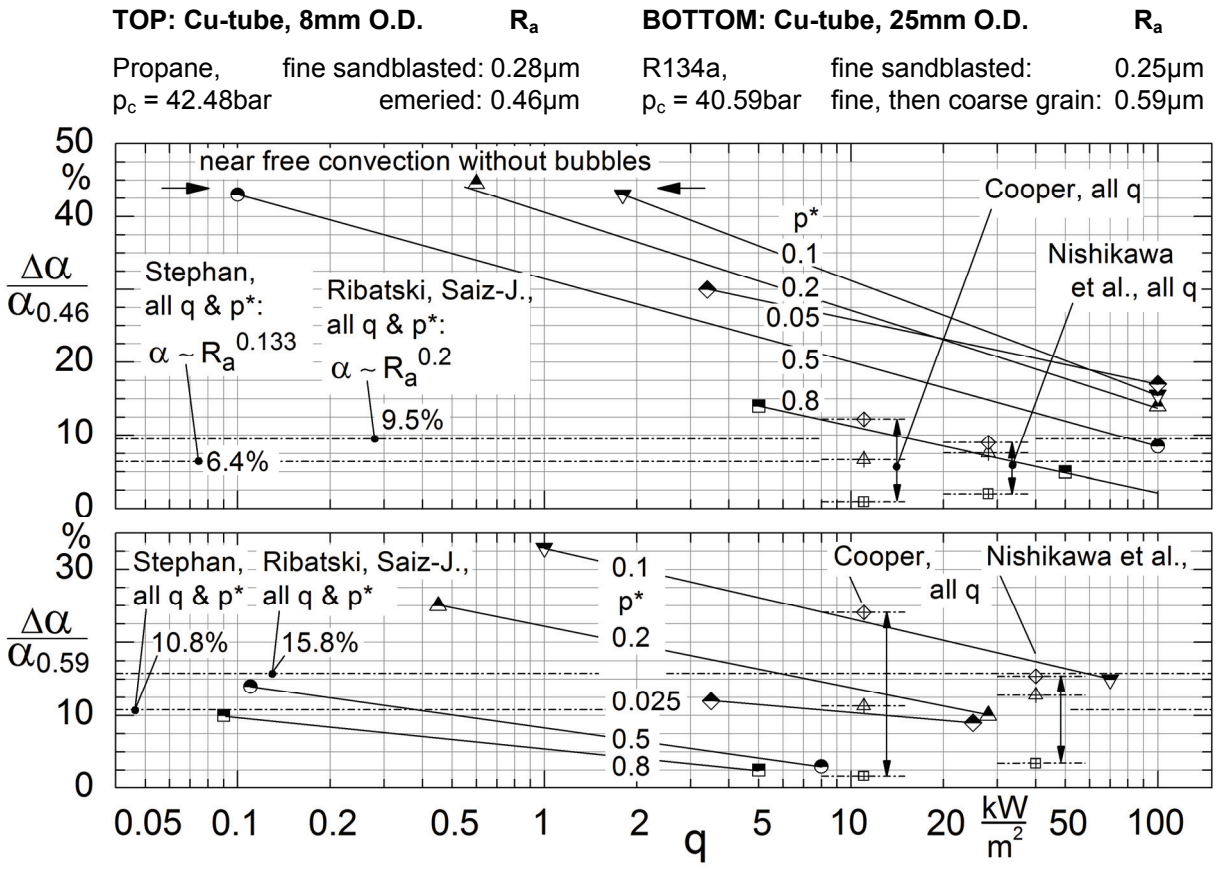
TOP: Cu-tube, 8mm O.D. Ra
Propane, fine sandblasted: 0.28µm
pc = 42.48bar emeried: 0.46µm
BOTTOM: Cu-tube, 25mm O.D. Ra
R134a, fine sandblasted: 0.25µm
pc = 40.59bar fine, then coarse grain: 0.59µm
near free convection without bubbles
Cooper, all q
p*
0.1
0.2
0.05
0.5
0.8
Nishikawa et al., all q
Stephan, all q & p*:
α ~ Ra 0.133
Ribatski, Saiz-J., all q & p*:
α ~ Ra 0.2
9.5%
6.4%
Δα / α0.46
50 % 40 20 10 0
Stephan, all q & p*
Ribatski, Saiz-J., all q & p*
10.8%
15.8%
0.1
p*
0.2
0.025
0.5
0.8
Cooper, all q
Nishikawa et al.,
Δα / α0.59
30 % 10 0
0.05 0.1 0.2 0.5 1 2 q 5 10 20 kW/m2 50 100

Figure 8

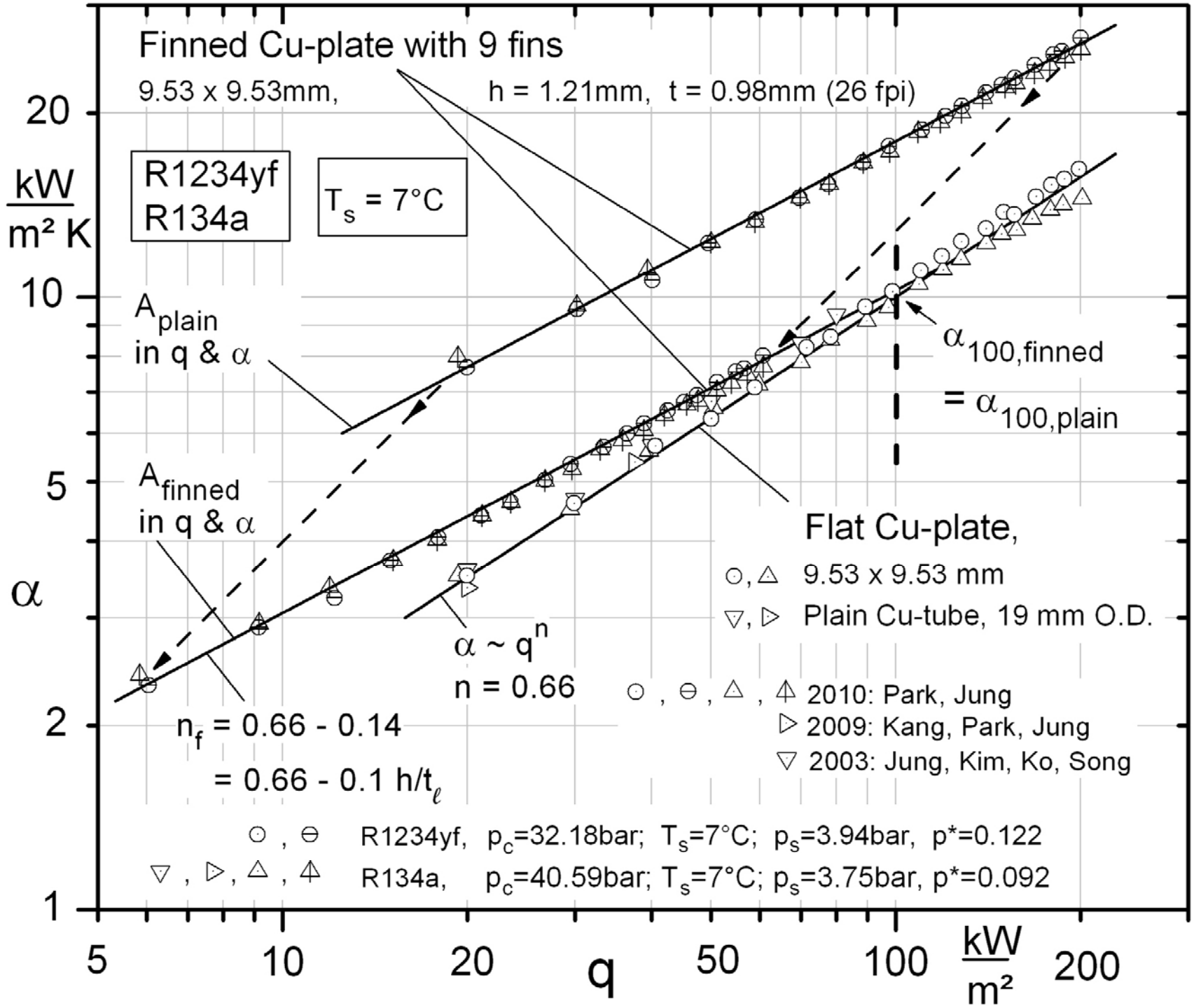
Finned Cu-plate with 9 fins
9.53 x 9.53mm,
h = 1.21mm, t = 0.98mm (26 fpi)
R1234yf
R134a
T_s = 7°C
$\frac{kW}{m^2 K}$
20
10
5
2
1
α
A_{plain} in q & α
A_{finned} in q & α
$\alpha_{100,finned}$ = $\alpha_{100,plain}$
Flat Cu-plate,
○, △ 9.53 x 9.53 mm
▽, ▷ Plain Cu-tube, 19 mm O.D.
α ~ q^n
n = 0.66
n_f = 0.66 - 0.14
= 0.66 - 0.1 h/t_ℓ
○ , ⊖ , △ , ⏃ 2010: Park, Jung
▷ 2009: Kang, Park, Jung
▽ 2003: Jung, Kim, Ko, Song
○ , ⊖ R1234yf, p_c=32.18bar; T_s=7°C; p_s=3.94bar, p*=0.122
▽ , ▷, △ , ⏃ R134a, p_c=40.59bar; T_s=7°C; p_s=3.75bar, p*=0.092
5
10
20
q
50
100
$\frac{kW}{m^2}$
200

Figure 9

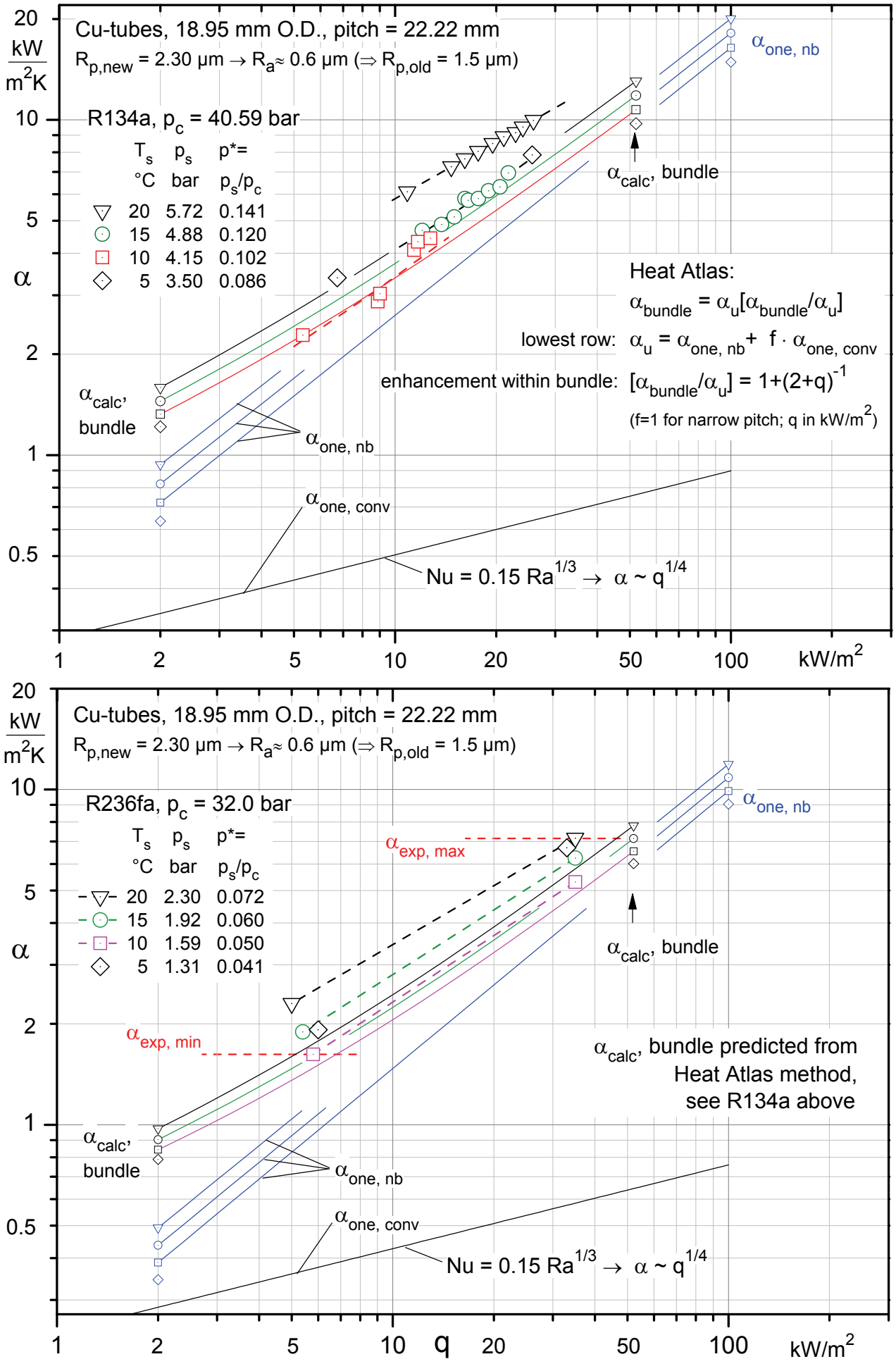
Cu-tubes, 18.95 mm O.D., pitch = 22.22 mm
$R_{p,new}$ = 2.30 µm → R_a≈ 0.6 µm (⇒ $R_{p,old}$ = 1.5 µm)
R134a, p_c = 40.59 bar
T_s °C | p_s bar | p*= p_s/p_c
20 | 5.72 | 0.141
15 | 4.88 | 0.120
10 | 4.15 | 0.102
5 | 3.50 | 0.086
Heat Atlas:
$\alpha_{bundle} = \alpha_u[\alpha_{bundle}/\alpha_u]$
lowest row: $\alpha_u = \alpha_{one,\,nb} + f \cdot \alpha_{one,\,conv}$
enhancement within bundle: $[\alpha_{bundle}/\alpha_u] = 1+(2+q)^{-1}$
(f=1 for narrow pitch; q in kW/m²)
$\alpha_{one,\,nb}$
α_{calc}, bundle
$\alpha_{one,\,conv}$
Nu = 0.15 $Ra^{1/3}$ → α ~ $q^{1/4}$
α
kW/m²K
q
kW/m²
Cu-tubes, 18.95 mm O.D., pitch = 22.22 mm
$R_{p,new}$ = 2.30 µm → R_a≈ 0.6 µm (⇒ $R_{p,old}$ = 1.5 µm)
R236fa, p_c = 32.0 bar
T_s °C | p_s bar | p*= p_s/p_c
20 | 2.30 | 0.072
15 | 1.92 | 0.060
10 | 1.59 | 0.050
5 | 1.31 | 0.041
$\alpha_{exp,\,max}$
$\alpha_{exp,\,min}$
α_{calc}, bundle predicted from Heat Atlas method, see R134a above
$\alpha_{one,\,nb}$
α_{calc}, bundle
$\alpha_{one,\,conv}$
Nu = 0.15 $Ra^{1/3}$ → α ~ $q^{1/4}$

Figure 10

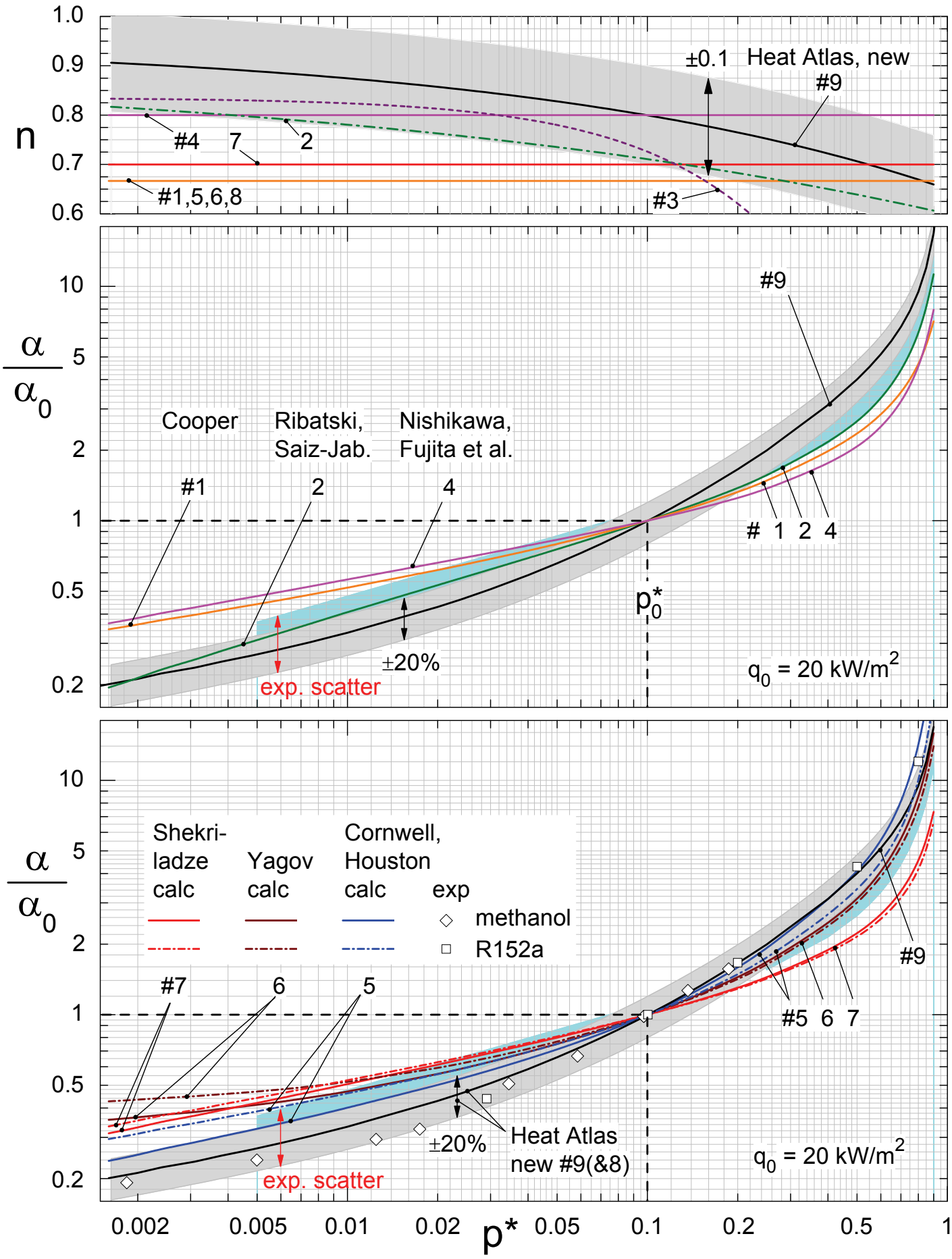
n
1.0
0.9
0.8
0.7
0.6
±0.1
Heat Atlas, new
#9
#4
7
2
#1,5,6,8
#3
α/α0
10
5
2
1
0.5
0.2
#9
Cooper
Ribatski,
Saiz-Jab.
Nishikawa,
Fujita et al.
#1
2
4
1 2 4
p*0
±20%
exp. scatter
q0 = 20 kW/m2
Shekri-
ladze
calc
Yagov
calc
Cornwell,
Houston
calc
exp
methanol
R152a
#7
6
5
#9
#5 6 7
±20%
Heat Atlas
new #9(&8)
exp. scatter
q0 = 20 kW/m2
0.002
0.005
0.01
0.02
p*
0.05
0.1
0.2
0.5
1

Figure 11

Jung et al.: T_s = 7 °C Cu-Tube, D = 19 mm, R_a = 0.35 µm

Shaded areas from new measurements for 23 fluids

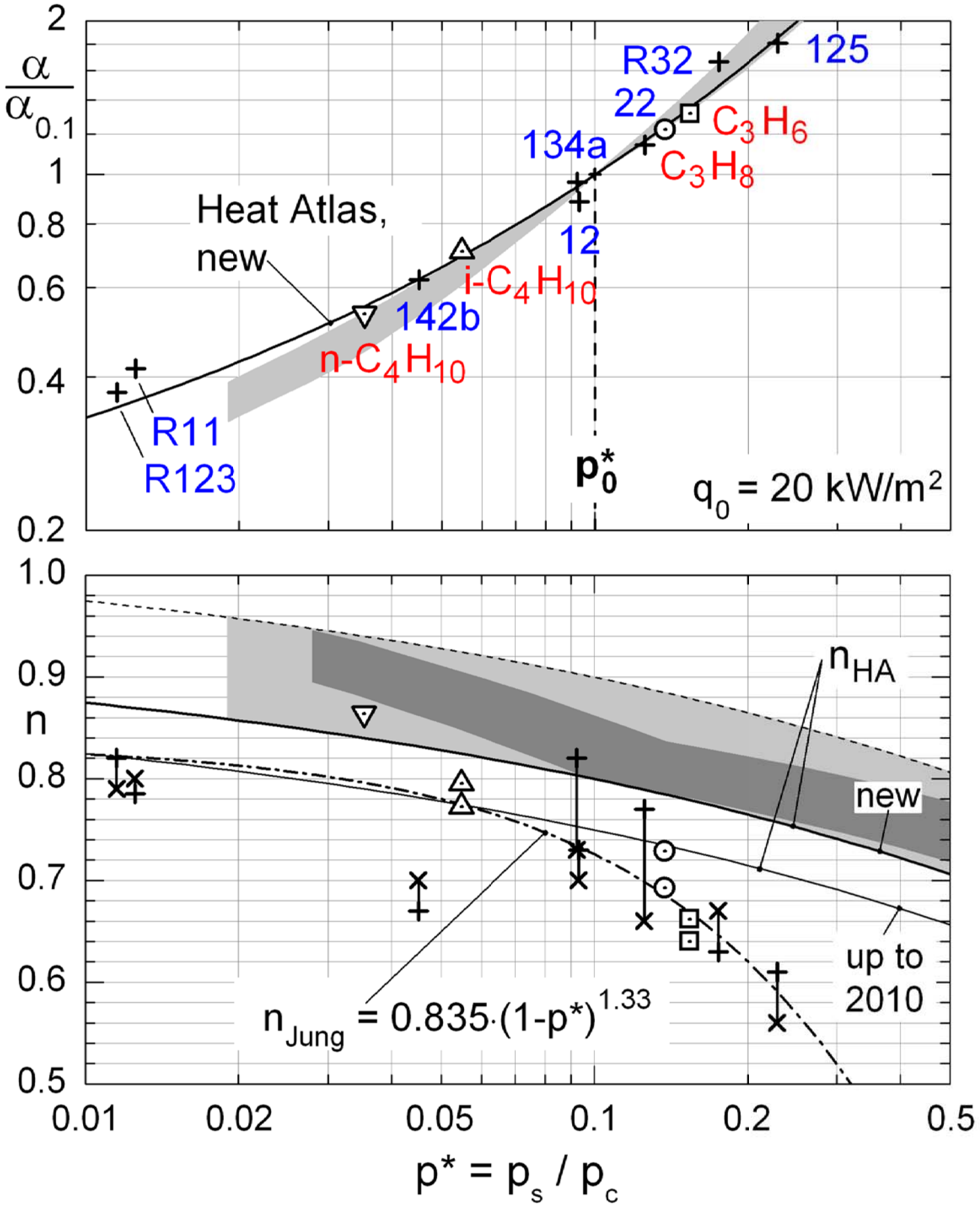

Figure 12

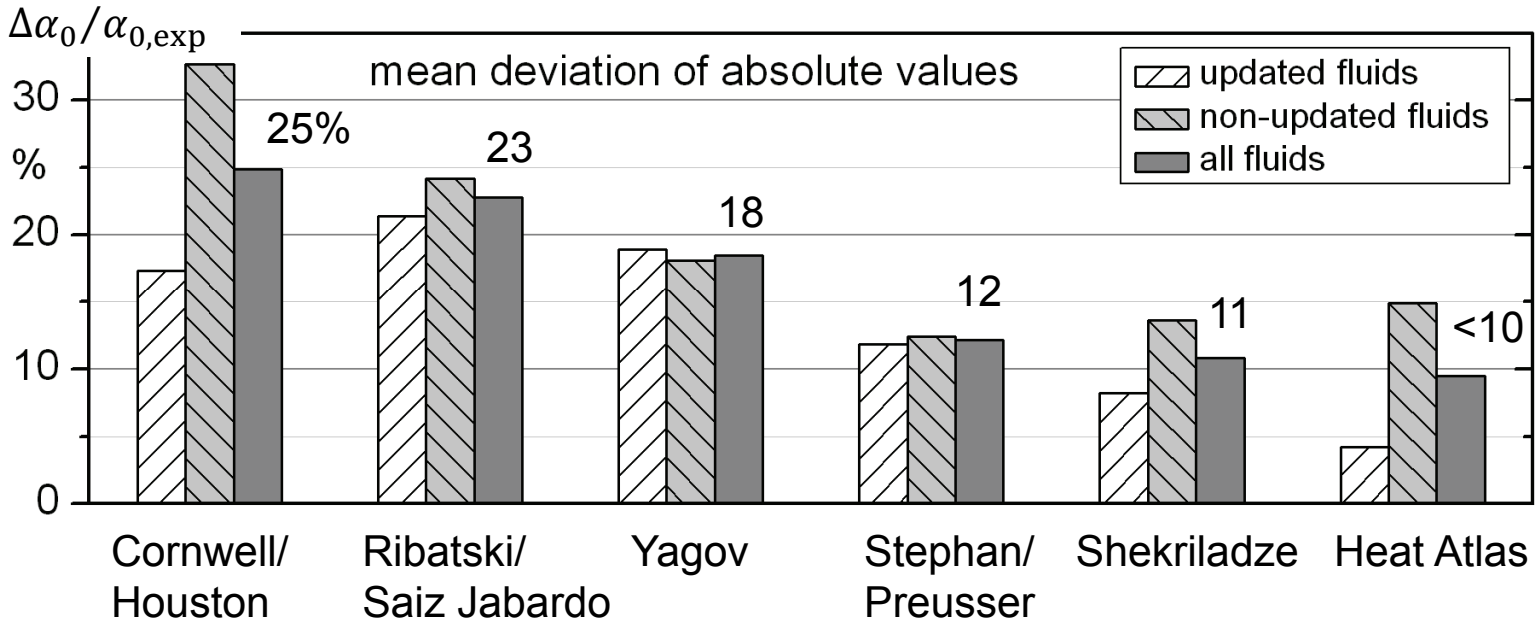
$\Delta\alpha_0/\alpha_{0,\mathrm{exp}}$
mean deviation of absolute values
updated fluids
non-updated fluids
all fluids
30
%
20
10
0
25%
23
18
12
11
<10
Cornwell/
Houston
Ribatski/
Saiz Jabardo
Yagov
Stephan/
Preusser
Shekriladze
Heat Atlas

Figure 13

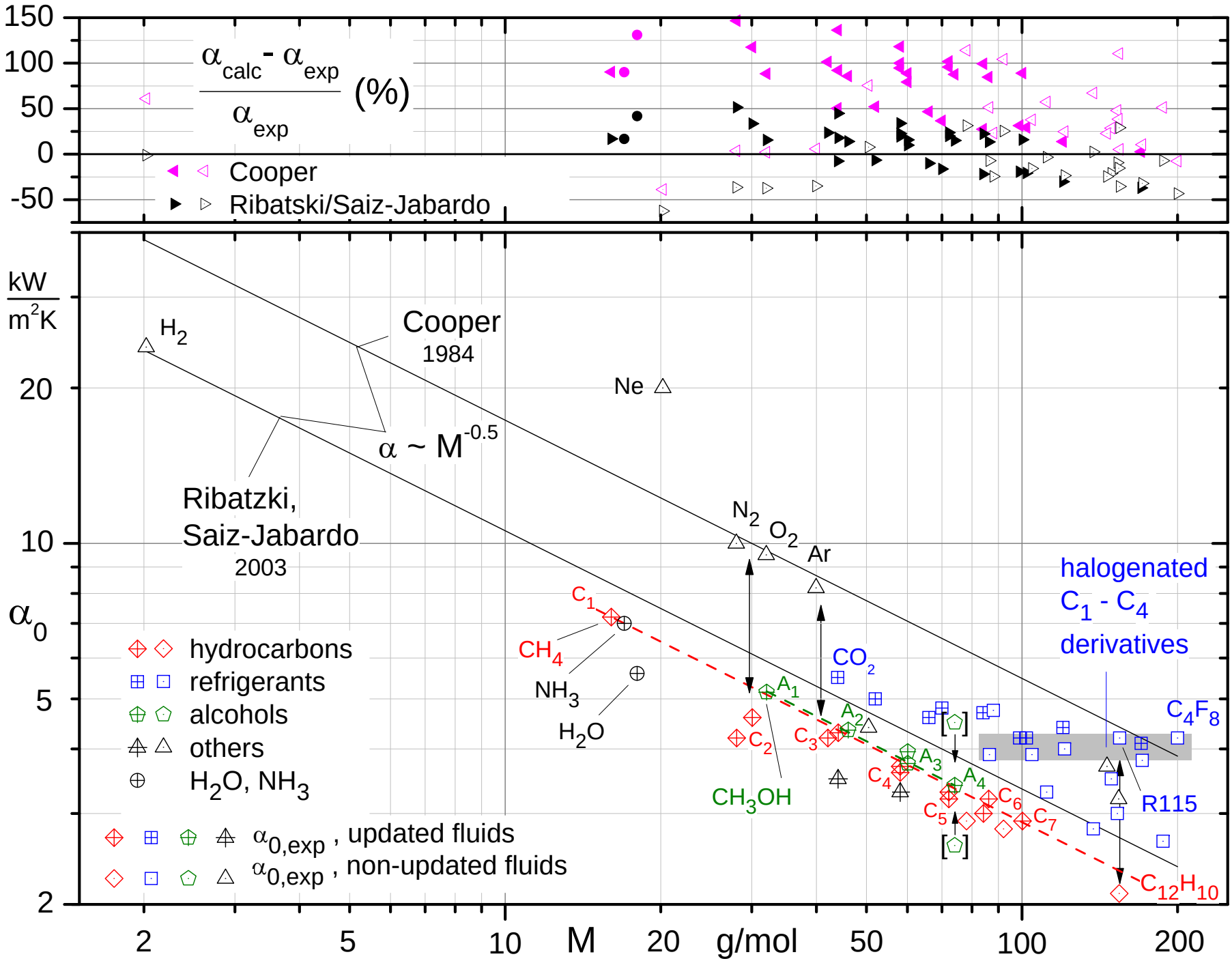
150
100
50
0
-50
$\frac{\alpha_{calc} - \alpha_{exp}}{\alpha_{exp}}$ (%)
Cooper
Ribatski/Saiz-Jabardo
kW / m²K
α_0
20
10
5
2
Cooper
1984
$\alpha \sim M^{-0.5}$
Ribatzki,
Saiz-Jabardo
2003
H2
Ne
N2
O2
Ar
CO2
CH4
NH3
H2O
CH3OH
C1
C2
C3
C4
C5
C6
C7
C12H10
A1
A2
A3
A4
[ ]
[ ]
halogenated
C1 - C4
derivatives
C4F8
R115
hydrocarbons
refrigerants
alcohols
others
H2O, NH3
α0,exp , updated fluids
α0,exp , non-updated fluids
2
5
10
M
20
g/mol
50
100
200

Figure 14

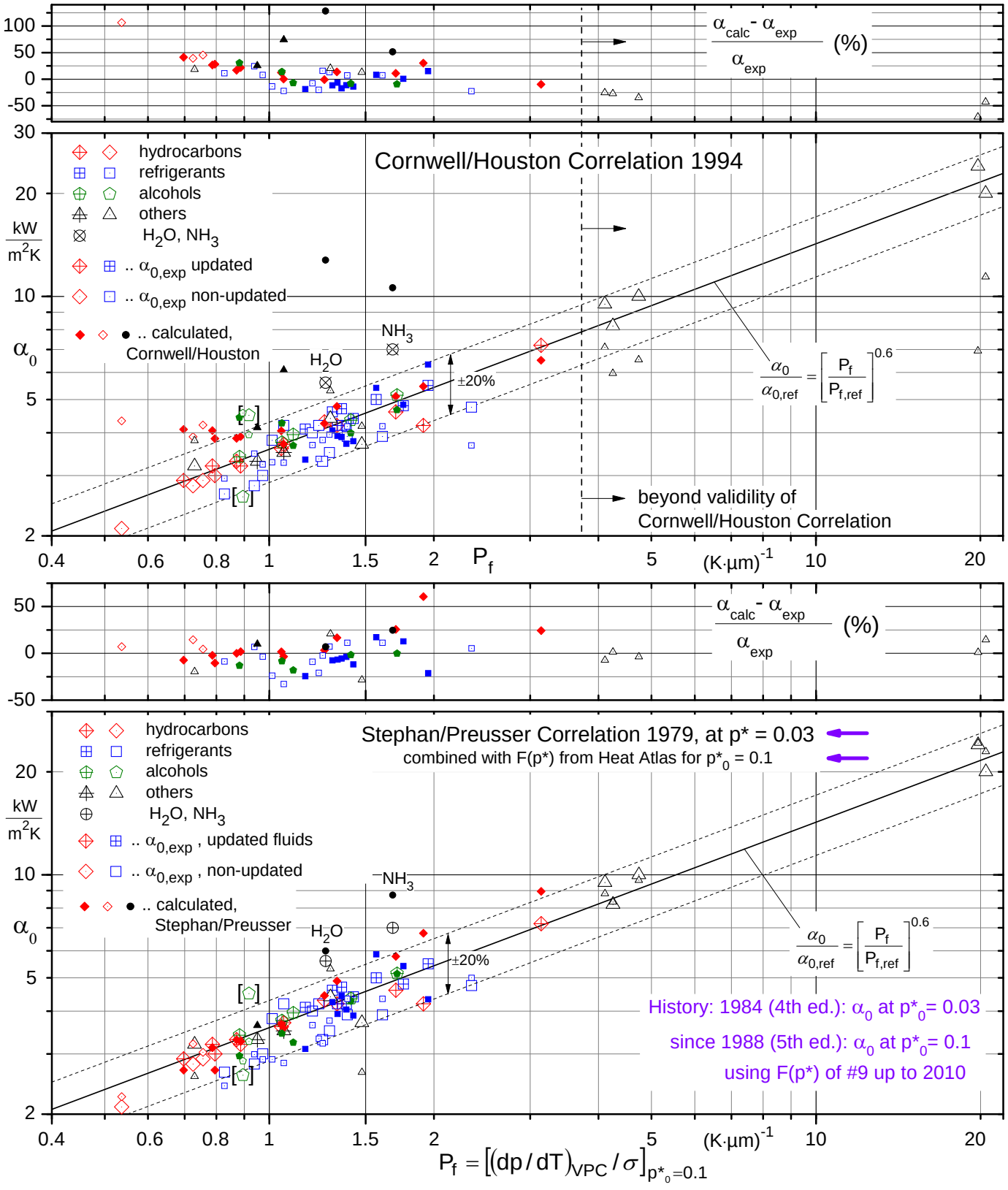
100
50
0
-50
$\frac{\alpha_{calc} - \alpha_{exp}}{\alpha_{exp}}$ (%)
30
20
10
5
2
kW/m²K
α_0
hydrocarbons
refrigerants
alcohols
others
H_2O, NH_3
.. $\alpha_{0,exp}$ updated
.. $\alpha_{0,exp}$ non-updated
.. calculated, Cornwell/Houston
Cornwell/Houston Correlation 1994
NH_3
H_2O
±20%
$\frac{\alpha_0}{\alpha_{0,ref}} = \left[\frac{P_f}{P_{f,ref}}\right]^{0.6}$
beyond validity of Cornwell/Houston Correlation
0.4
0.6
0.8
1
1.5
2
P_f
5
(K·µm)$^{-1}$
10
20
50
0
-50
$\frac{\alpha_{calc} - \alpha_{exp}}{\alpha_{exp}}$ (%)
20
10
5
2
kW/m²K
α_0
hydrocarbons
refrigerants
alcohols
others
H_2O, NH_3
.. $\alpha_{0,exp}$, updated fluids
.. $\alpha_{0,exp}$, non-updated
.. calculated, Stephan/Preusser
Stephan/Preusser Correlation 1979, at p* = 0.03
combined with F(p*) from Heat Atlas for p^*_0 = 0.1
NH_3
H_2O
±20%
$\frac{\alpha_0}{\alpha_{0,ref}} = \left[\frac{P_f}{P_{f,ref}}\right]^{0.6}$
History: 1984 (4th ed.): α_0 at p^*_0= 0.03
since 1988 (5th ed.): α_0 at p^*_0= 0.1
using F(p*) of #9 up to 2010
0.4
0.6
0.8
1
1.5
2
5
(K·µm)$^{-1}$
10
20
$P_f = [(dp/dT)_{VPC}/\sigma]_{p^*_0=0.1}$

Figure 15

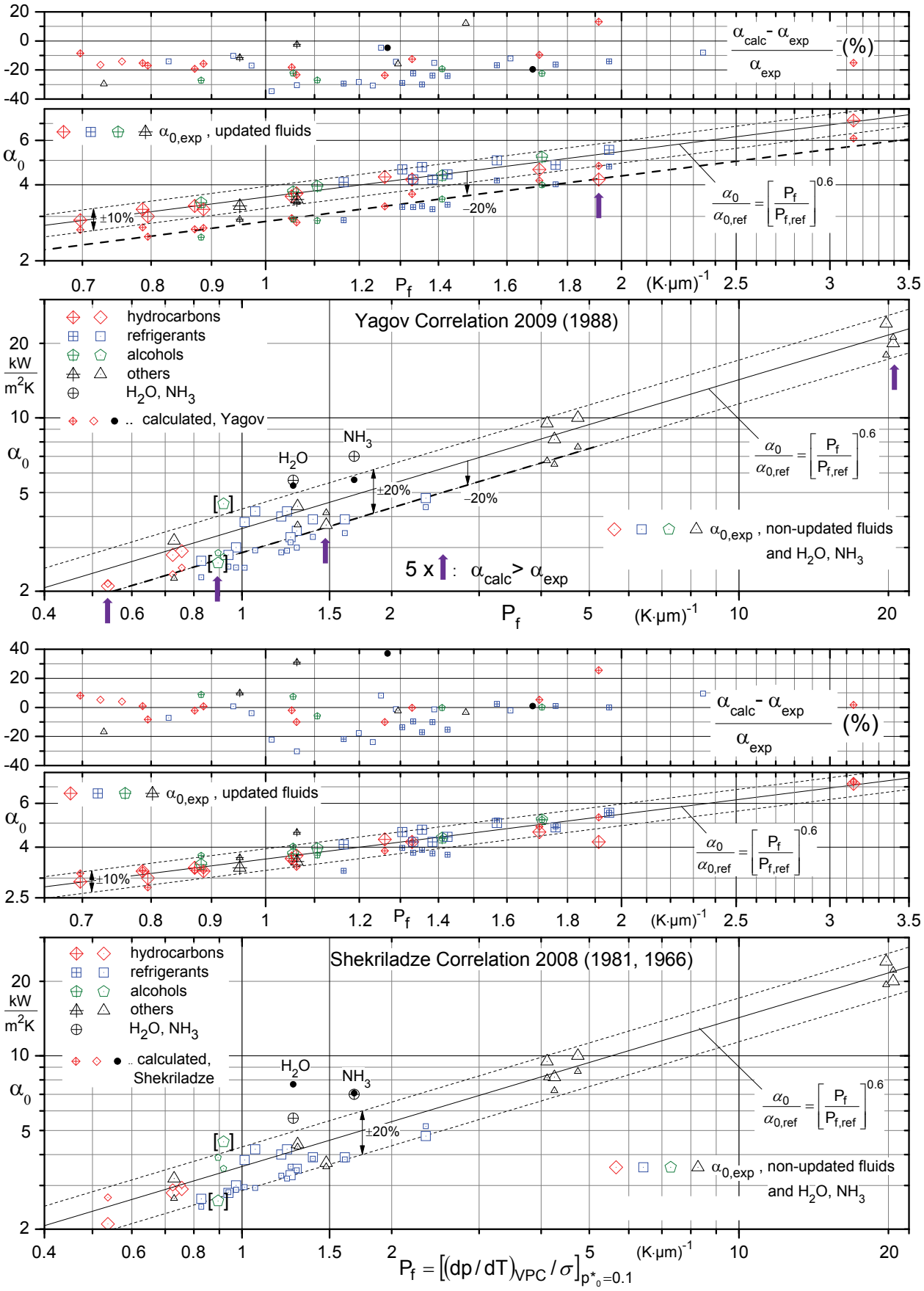
$\frac{\alpha_{calc} - \alpha_{exp}}{\alpha_{exp}}$ (%)
$\alpha_{0,exp}$, updated fluids
$\frac{\alpha_0}{\alpha_{0,ref}} = \left[\frac{P_f}{P_{f,ref}}\right]^{0.6}$
±10%
-20%
α_0
P_f
$(K \cdot \mu m)^{-1}$
Yagov Correlation 2009 (1988)
hydrocarbons
refrigerants
alcohols
others
H_2O, NH_3
.. calculated, Yagov
NH_3
H_2O
±20%
-20%
$\alpha_{0,exp}$, non-updated fluids and H_2O, NH_3
5 x : $\alpha_{calc} > \alpha_{exp}$
$\frac{kW}{m^2K}$
Shekriladze Correlation 2008 (1981, 1966)
calculated, Shekriladze
$P_f = [(dp/dT)_{VPC}/\sigma]_{p^*_0=0.1}$

Figure 16

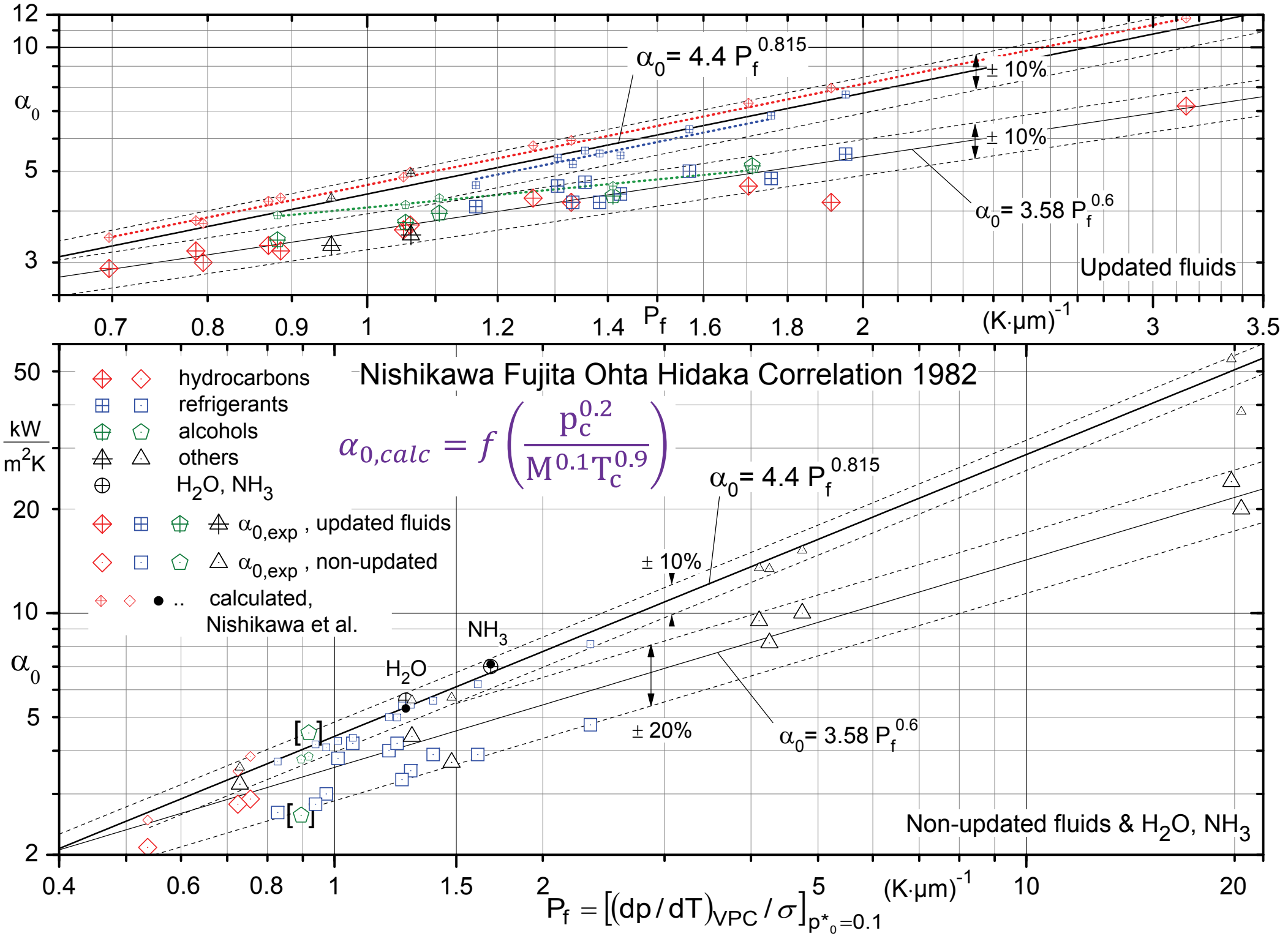
Updated fluids
$\alpha_0 = 4.4\ P_f^{0.815}$
$\alpha_0 = 3.58\ P_f^{0.6}$
± 10%
± 10%
α_0
P_f
$(K \cdot \mu m)^{-1}$
Nishikawa Fujita Ohta Hidaka Correlation 1982
$\alpha_{0,calc} = f\left(\frac{p_c^{0.2}}{M^{0.1} T_c^{0.9}}\right)$
hydrocarbons
refrigerants
alcohols
others
H_2O, NH_3
$\alpha_{0,exp}$, updated fluids
$\alpha_{0,exp}$, non-updated
calculated, Nishikawa et al.
NH_3
H_2O
± 20%
Non-updated fluids & H_2O, NH_3
$\frac{kW}{m^2K}$
$P_f = [(dp/dT)_{VPC} / \sigma]_{p^*_0=0.1}$

Figure 17

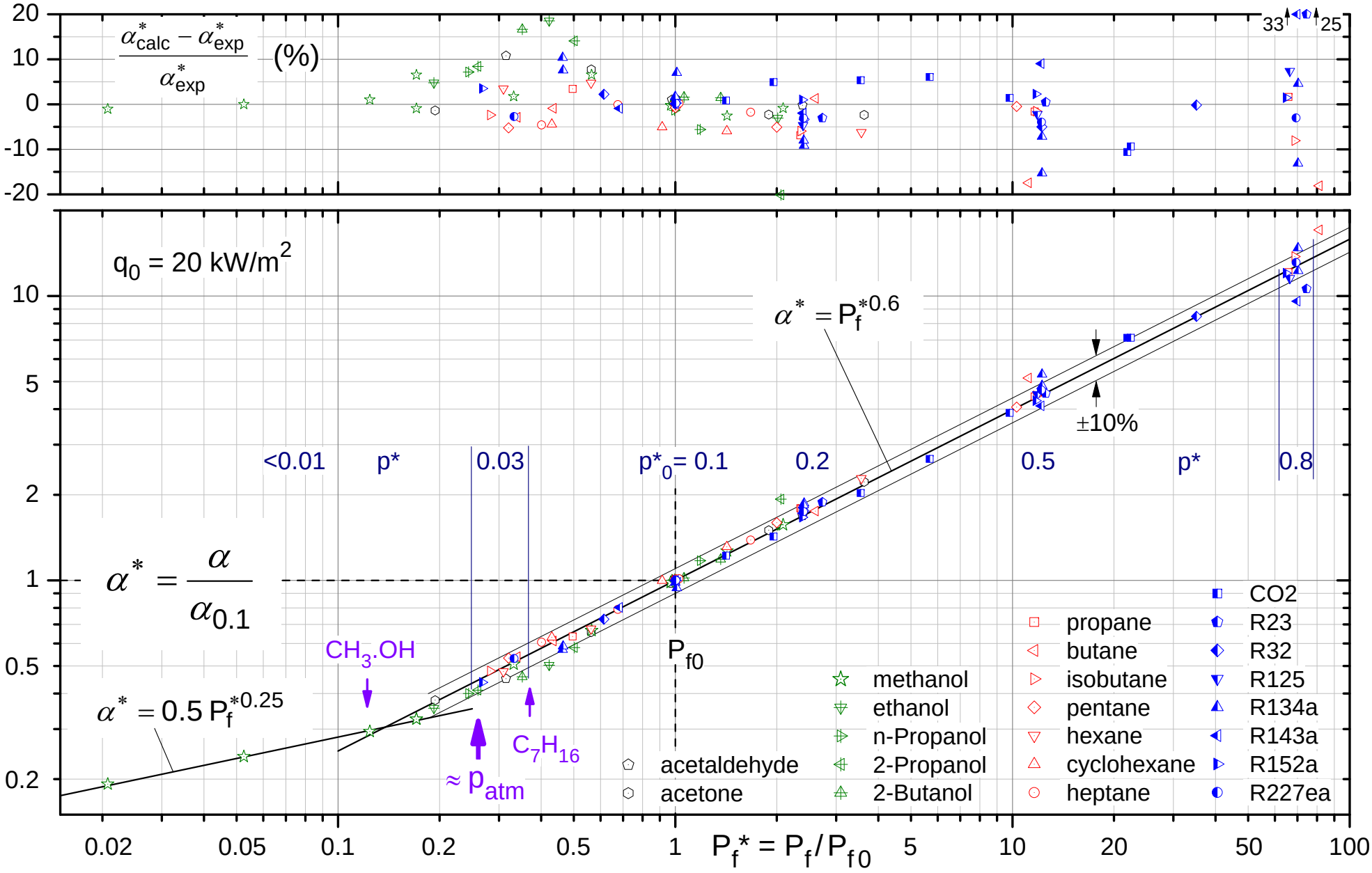
$\frac{\alpha^*_{calc} - \alpha^*_{exp}}{\alpha^*_{exp}}$ (%)
33
25
q_0 = 20 kW/m^2
$\alpha^* = P_f^{*0.6}$
±10%
<0.01
p*
0.03
p^*_0= 0.1
0.2
0.5
p*
0.8
$\alpha^* = \frac{\alpha}{\alpha_{0.1}}$
$\alpha^* = 0.5\, P_f^{*0.25}$
$CH_3.OH$
P_{f0}
$\approx p_{atm}$
C_7H_{16}
methanol
ethanol
n-Propanol
2-Propanol
2-Butanol
acetaldehyde
acetone
propane
butane
isobutane
pentane
hexane
cyclohexane
heptane
CO2
R23
R32
R125
R134a
R143a
R152a
R227ea
$P_f^* = P_f / P_{f0}$

Figure 18

Table 1. Selection of prediction methods for nucleate pool boiling heat transfer

1	Cooper (1984)	$\alpha = C_w \cdot M^{-0.5} \cdot p^{*(0.12-0.2\lg R_{p,old})} \cdot (-\log p^*)^{-0.55} \cdot q^{0.67}$, $with \quad q\ in\ W/m^2$, $C_w = 95/55$ for copper/stainless steel, and $R_{p,old} = R_a/0.4 \quad in\ \mu m$,
2	Ribatski, SaizJabardo (2003)	$\alpha = C_w \cdot M^{-0.5} \cdot p^{*0.45} \cdot (-log\ p^{*-0.8}) \cdot Ra^{0.2} \cdot q^m$, $with \quad m = 0.9 - 0.3\,p^{*0.2}, q\ in\ W/m^2, R_a\ in\ \mu m$ $and\ C_w = 100/110/85\ for\ copper/brass/stainless\ steel$
3	Jung, Lee, Bae, Oho (2004)	$\alpha = 41.4\ \frac{\lambda_\ell}{d_b}\left(\frac{\Delta\rho_{\ell g}}{\rho_\ell}\right)^{0.53} (-\log p^*)^{-1.52} \left(\frac{d_b q}{\lambda_\ell T_s}\right)^m$, $with \quad m = 0.835(1-p^*)^{1.33}$, d_b see #8
4	Nishikawa, Fujita, Ohta, Hidaka(1982)	$\alpha = 31.4\ \frac{{p_c}^{0.2}}{M^{0.1} \cdot {T_c}^{0.9}} \cdot F(p^*) \cdot G\left(R_{p,old}, p^*\right) \cdot q^{0.8}$, $with \quad F(p^*) = p^{*0.23}/(1-0.99p^*)^{0.9}$, $G = (8\,R_{p,old})^{0.2(1-p^*)}$, $q, p_c, T_c, M, R_{p,old} = R_a/0.4 \quad in \quad W/m^2, N/m^2, K, kg/kmol, \mu m$
5	Cornwell, Houston (1994)	$\alpha = 9.7\frac{\lambda_\ell}{D} \cdot F(p^*) \cdot {p_c}^{0.5} \left(\frac{\eta_\ell c_\ell}{\lambda_\ell}\right)^{0.4} \left(\frac{Dq}{\Delta h_{\ell g}\eta_\ell}\right)^{0.67}$, $F(p^*) = 1.8p^{*0.17} + 4p^{*1.2} + 10p^{*10}$, $p_c\ in\ bar$
6	Yagov (2009; 1988)	$\alpha = 0.07\left[\left(1 + \frac{\Delta h_{\ell g}}{2R}\frac{\Delta T}{{T_s}^2}\right)(1 + (1+800B)^{0.5} + 400B)\left(\frac{{\lambda_\ell}^2 \cdot q^2}{\nu_\ell\ \sigma\ T_s}\right)\right]^{1/3}$, $B = \frac{\Delta h_{\ell g}(\nu_\ell\,\rho_g)^{1.5}}{\sigma(\lambda_\ell \cdot T_s)^{0.5}}$, $\Delta T = 5K\ for\ \alpha_0(q_0, p_0^*)$
7	Shekriladze (2008, 1981,1966)	$\alpha = 0.0122\ \frac{\lambda_\ell}{r_0} \cdot {Re_{Sh}}^{0.25} \cdot \left(\frac{{r_0}^2 \rho_g \Delta h_{\ell g} q}{\sigma\ \lambda_\ell T_s}\right)^{0.7}$, $with \quad Re_{Sh} = \frac{\left[p\left(\rho_g^{-1} - \rho_\ell^{-1}\right)\right]^{0.5} \cdot \sigma c_\ell \rho_\ell^2 T_s}{\eta_\ell \Delta h_{\ell g}^2 \rho_g^2}$ $r_0 = 6\ \mu m\ for\ \alpha_0(q_0, p_0^*)$
8	Stephan, Preusser (1979), p*=0.03 & F(p*) of # 9	$\alpha = \frac{0.1\lambda_\ell}{d_b}\left[\frac{\rho_g}{\rho_\ell}\right]^{0.156}\left[\frac{\eta_\ell c_\ell}{\lambda_\ell}\right]^{-0.162}\left[\frac{\lambda_\ell^2}{\rho_\ell c_\ell^2 \sigma d_b}\right]^{0.35}\left[\frac{\Delta h_{\ell g} d_b^2 \rho_\ell^2 c_\ell^2}{\lambda_\ell^2}\right]^{0.371}\left[\frac{d_b\ q}{\lambda_\ell T_s}\right]^{0.674}$, $d_b = 0.146\beta\left[\frac{2\sigma}{g\Delta\rho_{\ell g}}\right]^{0.5}$ $\beta = 45^\circ(water); 1^\circ(cryogens), 35^\circ(other\ fluids)$
9	VDI Heat Atlas Gorenflo, Kenning (2010)	$\frac{\alpha}{\alpha_{ref}} = F(q) \cdot F(p^*) \cdot F_f(p^* = p_0^*) \cdot F_w$, $with\ F(q) = \left(\frac{q}{q_0}\right)^{n(p^*)}, F(p^*) = 0.7p^{*0.2} + 4p^* + \frac{1.4p^*}{1-p^*}$, $n = 0.95 - 0.3p^{*0.3}$ $F_w = F_R F_M = \left[\frac{R_a}{R_{a0}}\right]^{2/15}\left[\frac{(\lambda\rho c)_w}{(\lambda\rho c)_{Cu}}\right]^{0.25}$; $F_f(p_0^*) = \left[\frac{P_{f0}}{P_{fref}}\right]_{p_0^*=0.1}^{0.6}$, $P_f = \frac{(dp/dT)_{VPC}}{\sigma}$, $\alpha_{ref} = 3.58\ kW/m^2\,K \quad at\ P_{f,ref} = 1(K \cdot \mu m)^{-1}, q_0 = 20kW/m^2, p_0^* = 0.1, R_{a0} = 0.4\mu m, \quad wall: Cu$

Table 2. Mean relative deviations of calculated from experimental α_0-values for updated / non updated / all fluids of Table 3

		Cooper	Cornwell, Houston	Ribatski, Saiz Jabardo	Yagov	Stephan, Preusser	Shekriladze	Heat Atlas
		#1	*5*	*2*	*6*	*8*	*7*	*9*
UPDATED FLUIDS (number)		28	28	28	28	27	28	28
positive sign		28	17	19	1	11	14	15
negative sign		0	11	9	27	16	14	13
RMS	**%**	**85.9**	**22.7**	**23.8**	**20.0**	**17.1**	**11.4**	**6.4**
mean absolute value	**%**	**78.2**	**17.3**	**21.4**	**18.9**	**11.8**	**8.2**	**4.2**
NON-UPDATED (number)		27	27	27	27	27	27	27
positive sign		25	16	8	4	15	10	15
negative sign		2	11	19	23	12	17	12
RMS	**%**	**65.6**	**44.4**	**28.7**	**20.6**	**15.3**	**18.2**	**17.3**
mean absolute value	**%**	**51.8**	**32.7**	**24.2**	**18.1**	**12.4**	**13.6**	**14.9**
ALL FLUIDS (number)		55	55	55	55	54	55	55
positive sign		53	33	27	5	26	24	30
negative sign		2	22	28	50	28	31	25
RMS	**%**	**76.6**	**35.0**	**26.3**	**20.3**	**16.2**	**15.1**	**13.0**
mean absolute value	**%**	**65.2**	**24.9**	**22.8**	**18.5**	**12.1**	**10.8**	**9.5**

Table 3. Relative deviations (%) of calculated from experimental α_0-values at q_0^*, p , R_{a0} on copper heaters for the fluids of the Heat Atlas data bank

Updated fluids	α_0,exp. kW/m^{2}K	Cooper	Cornwell, Houston	Ribatski, Saiz Jabardo	Yagov	Stephan, Preusser	Shekriladze	Heat Atlas
Methane	*7.20*	90.28	-9.60	16.81	-15.14	24.31	1.71	-1.11
Ethene	*4.20*	146.67	30.10	51.43	13.21	60.71	25.55	25.71
Ethane	*4.60*	117.61	11.00	33.48	-9.59	25.65	5.26	7.17
Propene	*4.20*	101.43	13.71	23.57	-12.52	16.67	-0.29	1.19
Propane	*4.30*	92.09	-1.02	17.91	-23.60	3.26	-10.14	-4.42
n-Butane	*3.60*	100.00	12.44	22.78	-18.08	1.67	-1.97	2.50
i-Butane	*3.70*	94.59	0.22	19.46	-23.22	-3.51	-9.97	0.27
n-Pentane	*3.30*	95.76	16.82	20.00	-19.18	0.00	-2.18	0.00
i-Pentane	*3.20*	101.88	21.78	23.75	-15.69	1.88	0.75	4.06
n-Hexane	*3.20*	84.69	26.78	13.44	-15.25	-2.19	0.91	-3.13
Cyclohexane	*3.00*	99.33	28.17	22.33	-17.00	-10.33	-8.27	4.00
n-Heptane	*2.90*	88.97	41.10	15.86	-8.59	-7.24	8.07	-0.69
Carbon dioxide	*5.50*	50.36	15.00	-7.64	-14.05	-21.27	0.00	-2.73
R23	*4.80*	36.67	0.58	-16.25	-16.33	12.71	0.94	4.58
R32	*5.00*	52.20	8.10	-6.60	-16.74	17.20	2.36	-6.20
R125	*4.40*	13.86	-14.14	-30.23	-24.11	-11.82	-15.32	0.68
R134a	*4.20*	29.29	-6.76	-20.71	-22.38	-6.67	-9.64	1.19
R143a	*4.70*	27.45	-17.36	-21.91	-30.00	-5.53	-17.06	-8.51
R152a	*4.60*	46.74	-11.76	-10.00	-28.98	-7.61	-13.67	-8.70
R227ea	*4.10*	2.68	-18.56	-37.07	-29.37	-24.39	-21.80	-4.39
R507, az.	*4.20*	31.43	-11.50	-19.29	-23.86	-3.81	-10.14	3.57
Methanol	*5.15*	88.35	-9.42	15.53	-22.39	-0.19	0.17	-4.08
Ethanol	*4.35*	85.75	-8.23	14.02	-19.29	-1.61	-0.28	1.15
n-Propanol	*3.75*	88.80	13.79	15.73	-22.16	-8.27	7.41	-1.33
2-Propanol	*3.95*	79.24	-7.06	9.87	-27.01	-17.97	-5.95	-3.80
2-Butanol	*3.40*	87.65	30.38	15.00	-27.15	-12.94	8.74	-2.35
Acetaldehyde	*3.50*	136.29	74.34	44.86	-2.34	-	31.09	6.00
Acetone	*3.30*	118.18	25.58	33.94	-11.45	10.00	9.94	5.15
Non-updated fluids								
Benzene	*2.90*	114.14	45.24	31.38	-14.21	4.48	4.00	4.48
Toluene	*2.80*	104.29	39.07	25.36	-16.46	14.64	5.29	5.36
Diphenyl	*2.10*	110.48	106.24	29.05	2.05	7.14	27.95	17.62
RC318	*4.20*	-7.62	-22.12	-43.33	-30.50	-32.86	-30.19	-11.67
R13B1	*3.50*	28.57	12.86	-21.14	-14.40	7.14	-1.20	19.14
R22	*3.90*	51.28	7.03	-7.18	-15.13	11.28	-1.41	11.79
R11	*2.80*	67.14	24.21	2.50	-10.29	6.79	0.75	23.21
R12	*4.00*	24.75	-8.00	-23.50	-28.30	-9.00	-17.75	-0.25
R13	*3.90*	37.69	7.10	-15.64	-12.03	11.28	-2.05	22.31
R14	*4.75*	23.16	-22.69	-24.42	-8.08	5.26	9.52	25.68
R123	*3.00*	48.00	7.70	-9.33	-16.97	-3.67	-3.97	17.33
R113	*2.65*	51.32	11.02	-7.17	-14.08	-8.68	-7.17	20.75
R114	*3.80*	10.53	-13.68	-32.11	-34.55	-23.95	-22.18	-5.00
R115	*4.20*	5.24	-20.14	-35.48	-30.67	-20.95	-23.81	-3.33
R502, az.	*3.30*	57.27	15.48	-3.33	-4.67	-2.42	8.21	24.24
n-Butanol	*2.60*	145.38	75.65	50.38	9.88	10.00	49.42	28.85
i-Butanol	*4.50*	41.78	-12.33	-13.11	-38.87	-27.56	-22.02	-24.44
CH_3Cl	*4.40*	75.45	20.55	7.73	-15.84	20.91	-2.41	-5.00
CCl_4	*3.20*	38.44	18.66	-15.31	-29.50	-19.38	-16.81	-7.50
SF_6	*3.70*	22.70	13.05	-24.59	12.19	-28.38	-3.46	22.16
Oxygen	*9.50*	2.11	-25.22	-37.37	-29.25	-7.16	-14.05	-12.00
Nitrogen	*10.00*	3.70	-34.59	-36.40	-23.79	-3.60	-13.50	-8.90
Argon	*8.20*	5.85	-27.24	-35.00	-20.71	1.59	-11.67	4.02
Neon	*20.00*	-38.90	-42.92	-62.55	5.70	14.60	10.72	9.45
Hydrogen	*24.00*	61.04	-71.09	-1.21	-25.27	1.13	-19.32	-10.54
Water	*5.60*	131.07	128.11	41.79	-4.82	6.96	37.11	-26.25
Ammonia	*7.00*	90.14	51.47	16.71	-19.63	24.71	0.94	-30.14